Memoirs of the Faculty of Engineering, Nagoya University
Vol. 29, No. 1. (1977)

PHOTOCONDUCTION PROCESSES IN POLYMERS

MASAYUKI IEDA, YOSHIAKI TAKAI and
TERUYOSHI MIZUTANI

Department of Electrical Engineering

(Received May 30, 1977)

CONTENTS

Abstract

Photoconduction processes in various polymers were discussed in the range from ultraviolet to infrared wavelength (180 nm ~ 3.2 μm).

The excitonic carrier generation was proposed for the ultraviolet excited photocurrent of the aromatic polymers used here (polyethylene terephthalate, polyethylene naphthalate, polyparaxylyrene, polystyrene and polycarbonate) from the experiments of the optical absorption and the photoluminescence. Photocarrier injections from metal electrodes were also observed in all polymers employed here (polyethlene, polyvinyl chloride, as well as the aromatic polymers). The study of photoinjections could give the contact barrier height and suggest the existence of surface states. Generally, electrons were more easily injected. In the visible and infrared wavelength range, the optical release of trapped electrons was observed. The photostimulated detrapping current (PS DC) analysis revealed that the molecular motion greatly contributed to the detrapping process.

The carrier transport in polymers is considered to be composed of the inter- and intramolecualr transports. The molecular motion was also found to enhance the intermolecular carrier transport in polyethylene around the glass transition temperature. Also the photocurrent was found to be either bulk limited or electrode limited. In polyethylene terephthalate, space charge limited photocurrents were observed if excited with strongly absorbed light at high intensity, but at low intensity photocurrents deviated from the theoretical space charge limited characteristics.

1. Introduction

Polymeric materials have made a great contribution to the improvement of the electrical insulation system and also to the miniaturization of electrical equipments. In addition to the traditional application as an insulator, another application as a photoconductor has recently been developed.

In spite of such wide practical uses, surprisingly little is well understood about the fundamental electrical properties of polymeric materials (electrical conduction and dielectric breakdown). For example, even the kind of carriers (ion or electron) is still obscure in many polymers. This is partly because very small currents in good insulators prevent the investigation of the electrical conduction under natural condition. The complex configuration (amorphous, semicrystalline or crystalline structure of polymers) and various impurites inevitably introduced during manufacturing processes, also make it more difficult to understand their fundamental electrical properties.

Photoexcitation is one of ways to avoid such difficulties. Some known types of carriers can be introduced into polymers by means of optical excitation at suitable energy. These carriers are well considered to be electronic in nature, so we can explain the phenomena under photoexcitation by electronic carriers. Besides,

high density of photo-excited carriers can make electrical signals (electric current and electromotive force etc.) large enough to discuss the effects of the chemical and physical structures (molecular conformation, crystallinity, substitution of chemical groups, etc.) on the electrical conduction.

Another advantage of the study of photoconduction originates from the following fact that the photon energy is much more controllable as compared with the other excitation source such as an electron beam, γ-ray and X-ray. When we use strongly absorbed light, photocarriers will be generated near the illuminated surface, which enable us to decide the sign of carriers (electron or hole). It is also possible to release carriers trapped in localized centers at various depth by illuminating at appropriate energy. This photostimulated detrapping current (PSDC) analysis can provide further significant information about the nature of traps in polymers. The contact phenomena of polymer-electrode interface have hardly been discussed in polymers. Photo-electrons will be injected from metal electrodes into polymer-electrode interface when illuminated at energy large enough to surmount the contact barrier. The analysis of the photoinjetion current can give very useful results on the contact phenomena.

Although the analysis of photoconduction has great advantage as mentioned above, not so many articles have been reported. Even among articles reported, there are conflicting experimental results on polyethylene terephthalate (PET)[1, 2] and polyvinyl chloride (PVC).[3)~5)] The purpose of this article is to elucidate mechanisms of photoconduction in polymers. This is also of great help for the understanding of the fundamental electrical properties of polymers and to the improvement of the insulation properties.

2. Experimental Procedures

2. 1. Specimen

Specimens investigated are commercial films, which are summarized in Table 1. Polyethylene are nominally free of additives and antioxidants.

Thin Au electrode of 3 cm in diameter which transmits about 60 % of incident light in the wavelength range from 600 nm to 200 nm, was evaporated on one side of the specimen at 5×10^{-5} Torr. On the other side, a main electrode of the same size and a guard electrode were evaporated.

2. 2. Experimental Apparatus

2. 2. 1. Photoconductivity Measurements

The experimental apparatus for measurements of photoconduction is schematically shown in Fig. 1. A 500 *W* xenon lamp was used as an exciting source. The light beam focussed by a quartz lens was introduced into Bousch and Lomb high intensity monochromator with 4 interchangeable gratings shown in Table 2. Spurious light was removed by using suitable colored glass filters. In order to change light intensity, a neutral filter was used, which was a quartz plate with Au evaporated on its surface in suitable thickness.

The whole system can be evacuated to 10^{-5} Torr. The electrode system is shown in Fig. 2. A nickrome heater and liquid N_2 were used to control the temp-

Table 1. Specimens investigated.

Specimen	Code	Formula**	T_g(℃)	X_c(%)*	Thick-ness (μm)
polyethylene		$(-C-C-)_n$			
(low density)	LD-PE		−25	46	20
(high density)	HD-PE		−18	75	20
polypropyrene	PP	$(-C-C(-C)-)_n$	−13		20
ethylene-vinyl acetate copolymer	EVA	$[(-C-C-)_m-C(-O-C(=O)-C)-]_n$		18	20
polyvinyl chloride	PVC	$(-C-C(-Cl)-)_n$	80		20
polyethylene terephthalate	PET	$(-C-C-O-C(=O)-C_6H_4-C(=O)-O-)_n$	85	41	12, 6
polyethylene naphthalate	PEN	$(-C-C-O-C(=O)-C_{10}H_6-C(=O)-O-)_n$	110-120	45	12, 6
polypara-xylyrene	PPX	$(-C-C-C_6H_4-)_n$	60-70	37-51	12
polystyrene	PS	$(-C-C(-C_6H_5)-)_n$	84		28
polycarbonate	PC	$(-C_6H_4-C(-C)(-C)-C_6H_4-O-C(=O)-O-)_n$	147		35

*X_c: crystallinity, ** H is abbreviated.

Table 2. Performance of the gratings.

grating	UV	UV-V	IR-1	IR-2
wavelength (nm)	200-400	350-800	700-1600	1400-3200
braze wavelength (nm)	250	500	1000	2000
groove (lines/mm)	2700	1350	675	377.5
reciprocal linear dispersion (nm/mm)	3.2	6.4	12.8	25.6
resolution (nm)	2	5	10	20

effective apparture ratio f/3.5 forcal length 0.25 (m)

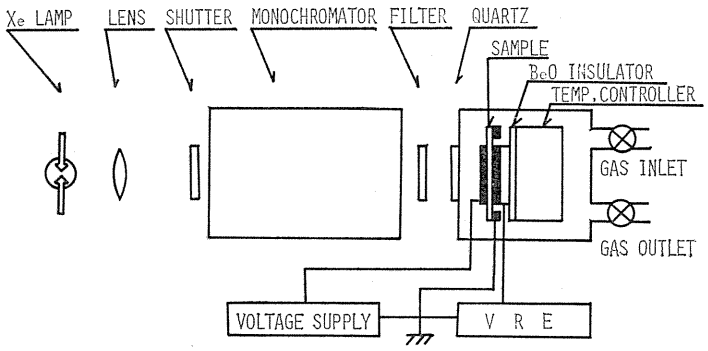

Fig. 1. Block diagram for measurements of photoconduction.

erature of the specimen from −185℃ to 200℃. The main electrode was electrically insulated by BeO ceramics. Electric currents were measured by a vibrating reed electrometer (VRE). Temperature of the specimen was controlled by a programable thyritor PID controller. Dry cells were used as a stable voltage source.

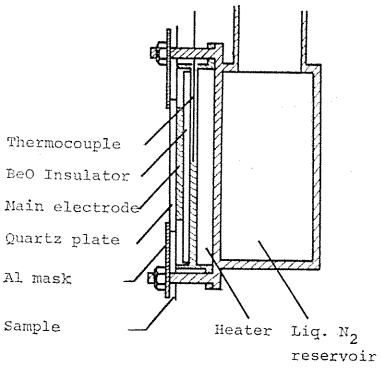

Fig. 2. Structure of electrode system.

2. 2. 2. Photoluminescence Measurement

Two sets of the monochromator were used to measure photoluminesence as shown in Fig. 3. The same light source of a 500 *W* xenon lamp was used in this measurement, but great care was paid to remove spurious light as possible. The

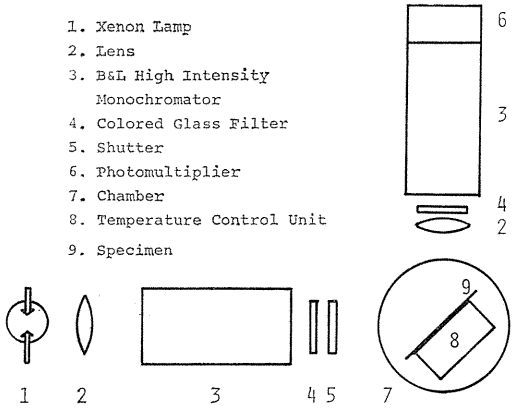

Fig. 3. Arrangement for measurements of photoluminescence.

emitted light was detected by a photomultipler (PM) through a filter and a monochromator. The PM was cooled to reduce the dark current noise. Since a whole system is the same as that used in the measurement of photoconduction, the simultaneous measurement of photoluminescence and photocurrent can be carried out at arbitrary temperature. Also simultaneous measurement of thermally stimulated current (TSC) and thermoluminescence was carried out with this system as mentioned in § 3. 2. 4. When we measured phosphorescence spectrum, a rotating phosphoroscope was used at 3240 Hz.

2. 2. 3. Optical Absorption Measurements

The optical absorption spectra of polymers are also of great importance for understanding the excited state of polymers. Aromatic polymers such as PET, polystyrene (PS) have so large absorption coefficients that commerical films are too thick to obtain the exact absorption spectra. Accordingly, we resolved commercial films into suitable solvents (trifluoroacetic acid for PET, ortochloro phenol for polyethylene naphthalate (PEN), and toluene for PS and polycarbonate (PC) and cast on a quartz plate in a few hundred Å thickness. The absorption spectra were obtained on these thin films by a spectrophotometer.

2. 3. Experimental Procedures

2. 3. 1. Photoconductivity Measurements

After setting the specimen, the whole system was evacuated to $\sim 10^{-3}$ Torr. When a voltage was applied to the specimen, a so-called absorption current was observed to decay for a long period, for example, half a day for PET. After the dark current reached a steady state, the photocurrent spetrum was measured by either scanning the wavelength of incident light or at a certain wavelength for 20 min. The letter is called here as the steady state photocurrent. All measurement were carried out on different films of specimen to avoid the hysteresis effect. In the case of PSDC measurements, the wavelength was varied step by step with an interval of 50 nm in substitution for the automatic scanning, because the photodetrapping current was so small that the signal might be buried in the noise or the drift of the dark current. The PSDC was sometimes measured by suppressing large dark currents.

2. 3. 2. Thermally Stimulated Current (TSC) and Thermoluminescence (TL) Measurements

Analyses of TSC and TL have often been applied to the study of traps in polymeric materials as well as in inorganic materials. The experimental procedure is shown in Fig. 4. At first, a photo-electret was formed at −185℃ by illuminating the specimen at a certain applied field E_p for 30 min. It was waited for 1 hour before starting the measurement of TSC and TL. The TSC and TL curves were measured by heating the specimen at a rate of 6 ℃/min. with no applied field.

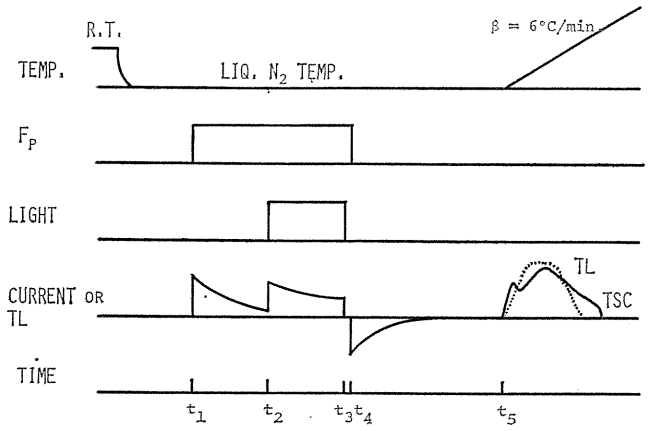

Fig. 4. Experimental procedure for measurements of TSC and TL.

3. Photoconduction Processes in Polymers

3. 1. Introduction

The study of photoconduction in polymers was started in 1956 by J. F. Fowler[6] who successfully explained the X-ray induced photoconduction (in a wide sense) in several polymers on the ground of the band conduction involving various traps. The study of photoconduction induced by ultraviolet or visible light was reported in 1961, and 1962 by G. Oster[7] and H. J. Wintle.[8] T. Tanaka[9] discussed infrared photocurrents observed in electron beam irradiated PE.

In this way, available wavelength is fairly wide from vacuum ultraviolet to infrared region. In many saturated polymers, photogeneration of an electron hole pair may be expected to be possible only by vacuum ultraviolet light having energy larger than 8 eV. Ultraviolet light having energy of $8 \sim 4$ eV can excite molecular groups such as benzene, and also inject carriers from electrodes or release carriers trapped by various localized centers.

In the following, several mechanisms of photoconduction in polymers will be discussed in the range from ultraviolet to infrared region.

3. 2. Photocarrier Generation Mechanism

3. 2. 1. Intrinsic Photocarrier Generation

Saturated hydrocarbons such as PE slightly absorb light in the ultraviolet range as shown in Fig. 5. Observed absorptions are considered to be ascribed to aromatic impurities[10] or oxidation products like carbonyl groups. In order to discuss the intrinsic absorption, we must use vacuum ultraviolet light ($\lambda < 180$ nm). Unfortunately, available wavelength in our experiment is limited to the region of ultraviolet longer than 180 nm. Photoconduction in the vacuum ultraviolet range has scarcely been studied as yet. Only a few reports[11, 12] have been presented to date. In this section, we will briefly review on the reported results in this wavelength range.

Optical absorption spectrum in the wavelength range shorter than 180 nm was

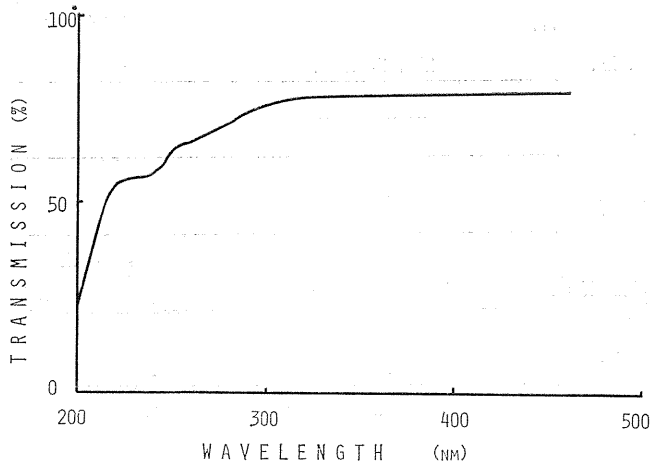

Fig. 5. Transmission spectrum for LD-PE (20 μm).

reported by Partridge[10], George[13] and Tanaka.[14] According to these results, optical density increases abruptly at 160 nm and remains constant (140 ~ 110 nm) and then sharply rises ($\lambda<110$ nm). The sharp rise observed at $\lambda<110$ nm is considered to indicate an ionization of PE molecules.[10]

The theoretical calculation of the band structure of PE has been conducted by many physicists[15, 16] who recognized the saturated linear polymers such as PE as a linear array of identical cells consisting of covalent bonds of simple atoms (C, H). Energy gap and ionization energy of PE obtained from these experiments and calculations are summarized in Table 3. It seems necessary for the intrinsic photo-

Table 3. Energy gap and ionization energy for PE.

	calculation				experimental results				
	Beveridge	Duke	Falk	Delhalle					
	INDO* MINDO**	SAMO	LCAO-LO M.F.T.	ab-initio	Fujihira	Tanaka	George	Partridge	Less
E_g (eV)	13.64* 9.56**	18.96	8.1	7.7	8	7.35	9	7.6	8.8
I_c (eV)		11.94	11.3	8.3	10			10	7.6-8.8

E_g: energy gap, I_c: ionization energy

carrier generation to illuminate PE at energy higher than ~ 8 eV. Less and Wilson[11] reported the intrinsic photocarrier generation in solution grown PE films. The threshold energy for the carrier generation was 8.8 eV which corresponds to the energy gap E_g. The photoresponse varied as $(h\nu-E_g)^2$ in the energy $h\nu$ larger than E_g. These authors reported also photoelectron emission from PE, the threshold energy of which was the same as that of photoconduction. From these results, they estimated the electron affinity and the ionization potential as 0 ~ 1.2 eV and 7.6 ~ 8.8 eV, respectively.

3. 2. 2. Excitonic Photocarrier Generation

The exciton induced photocarrier generation is reported in saturated hydrocarbons such as PE[11] as well as aromatic hydrocarbon PS[12] in the vacuum ultraviolet range. We have found also in the ultraviolet region the exciton induced photocarrier generation in other aromatic hydrocarbons such as PET, PEN, polyparaxylyrene (PPX) and PC. At first, the excited states of these polymers will be discussed from the results of optical absorption and luminescence studies.

1) Excited states

Optical absorption spectra of these aromatic polymers are shown in Figs. 6 ~ 10. Among these polymers, only PET and PEN have an extended conjugated system of benzene or naphthalene with COO groups. The optical absorption spectra of PS, PS and PPX were nearly the same as that of benzene itself, while those of PET, PEN showed a distinct red shift as compared with that of benzene or naphthalene. The red shift is considered to be the result of the extended conjugate system. The absorption spectra of substituted benzene were reported by Doub and Vandenbelt[17] and Nagakura and Tanaka. [18] According to these reports, benzene derivatives substituted by strongly interacting groups (NO_2, CHO, etc) show remarkable red shifts. Terephthalic acid and terephthalaldehydic acid which may be well considered to be model compounds for PET, show quite similar absorption spectra to that of PET as shown in Fig. 11. A similar result was reported on β-naphtyl aldehyde corresponding to PEN. Polymers such as PPX and PS and PC showed only a slight red shift which is explained from the interaction of σ electrons with π system in benzene. In this case, the red shift is considered to be much smaller than the case of COO substitution. A model compound for PPX, p-xylene (dimethyl

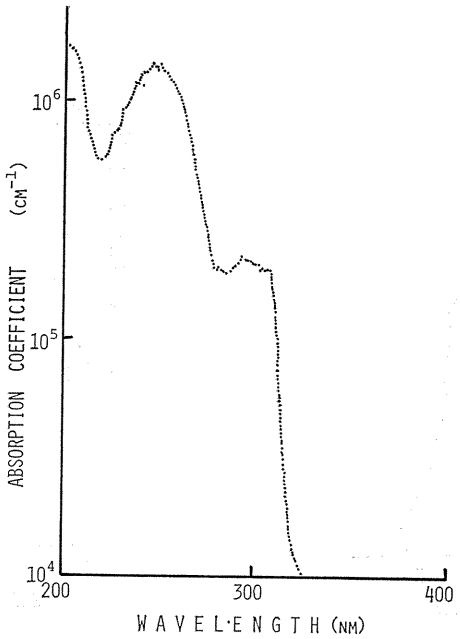

Fig. 6. Absorption coefficient of PET.

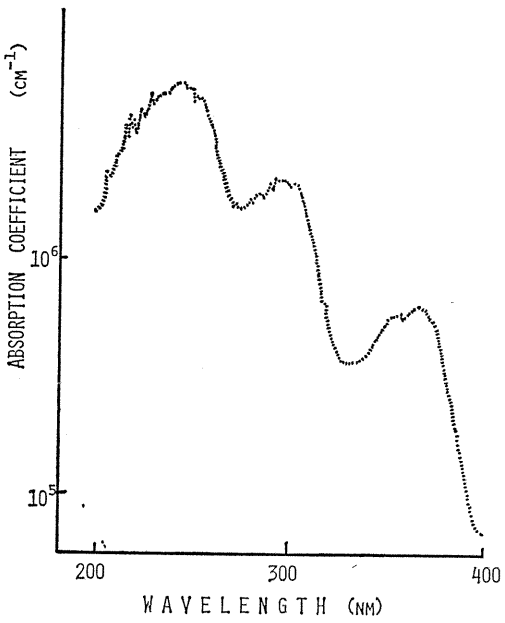

Fig. 7 Absorption coefficient of PEN.

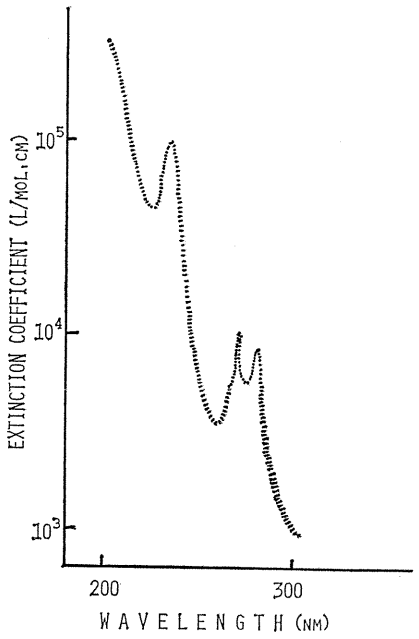

Fig. 8. Molar extinction coefficient of PPX.

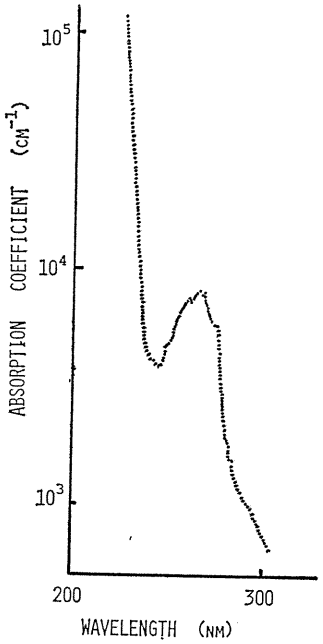

Fig. 9. Absorption coefficient of PS.

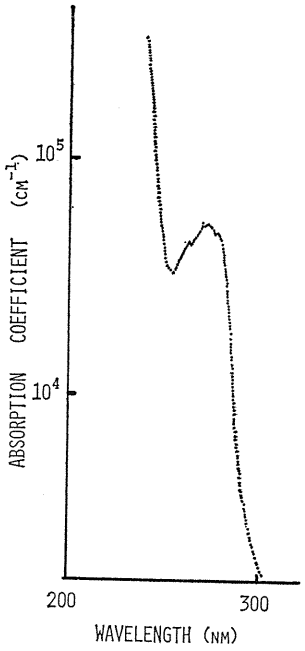

Fig. 10. Absorption coefficient of PC.

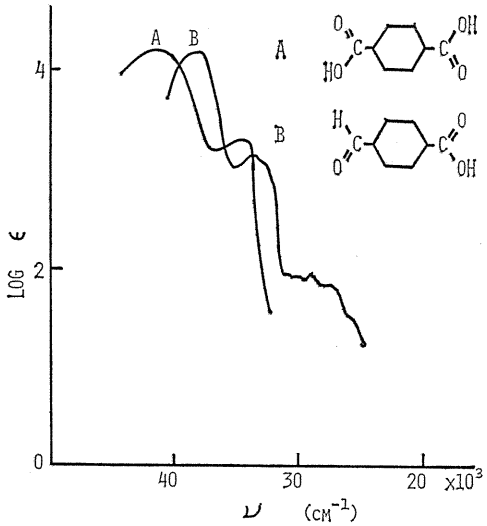

Fig. 11. Molar extinction coefficient in A : terephthalic acid, B : terephthaldehydic acid. (after R. N. Nurmukhametov et al.; Optics and Spectroscopy **24** (1968) 107).

substituted benzene) shows an absorption spectrum with a slight red shift of 1390 cm^{-1} for the 255 nm peak in benzene.[19] Also a model compound for PS, ethyl benzene ($C_6H_5C_2H_5$) shows only a 550 cm^{-1} red shift for the same peak.[19]

To summarize the interpretation of the observed absorption peaks in these aromatic hydrocarbons, they are considered to correspond to the π π^* transitions $^1B_{2u} \leftarrow\!\!- {}^1A_{1g}$, $^1B_{1u} \leftarrow\!\!- {}^1A_{1g}$ in benzene (or naphthalene for PEN), respectively as summarized in Table 4.

Table 4. Optical transitions in aromatic polymers and their model compounds.

	$^1E_{1u} \leftarrow {}^1A_{1g}$	$^1B_{1u} \leftarrow {}^1A_{1g}$	$^1B_{2u} \leftarrow {}^1A_{1g}$
benzene	183p	208o	263o
naphthalene	220p	275p	313o
β-naphthyl aldehyde	248p	236p	346o
p-xylene	193p	222p	270p
terephthalic acid	196p	230p	282p
PET	<200	260p	300p
PEN	244p	290p	380o
PPX	<200	230p	270p

o : onset, p : peak (nm)

These electronic structures of aromatic polymers can be also discussed from the photoluminescence study. Photoluminescence from polymers has scarcely been reported except for PS[20] and polyvinyl carbazole (PVK).[21] Typical results on several polymer films are shown in Figs. 12 ~ 15 (not corrected). Each excitation

wavelength was selected to the wavelength corresponding to the ${}^1B_{2u} \longleftarrow {}^1A_{1g}$ transition. All results were obtained at −185℃. In Figs. 12 and 13, phosphorescence

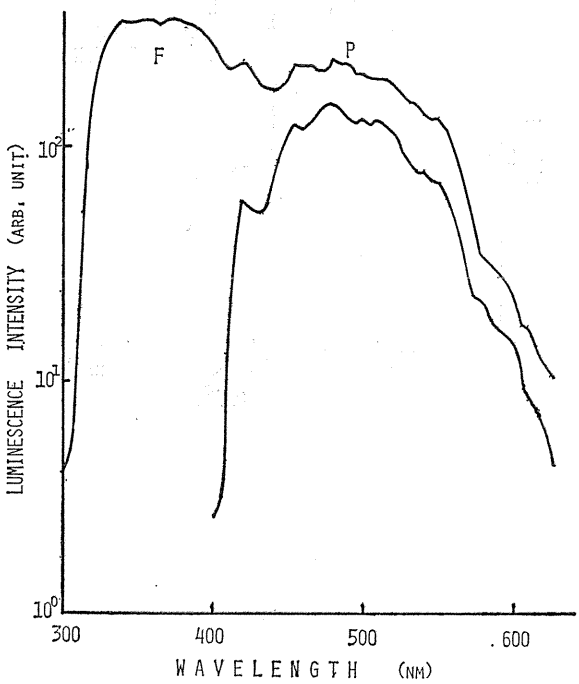

Fig. 12. Luminescence spectrum from PET, F : fluorescence, P : phosphorescence.

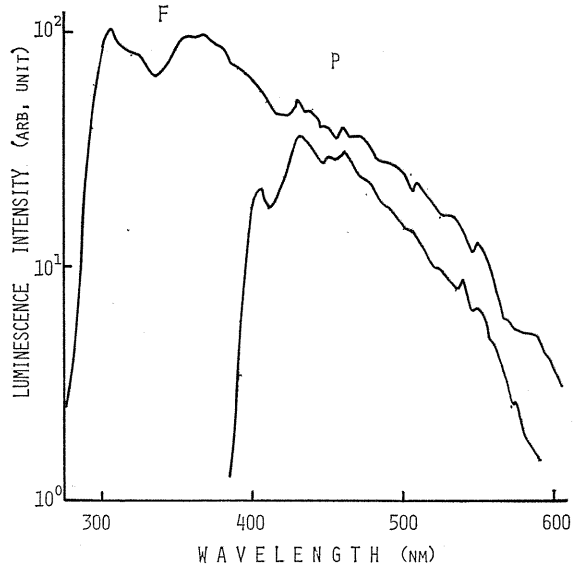

Fig. 13. Luminescence spectrum from PPX, F : fluorescence, P : phosphorescence.

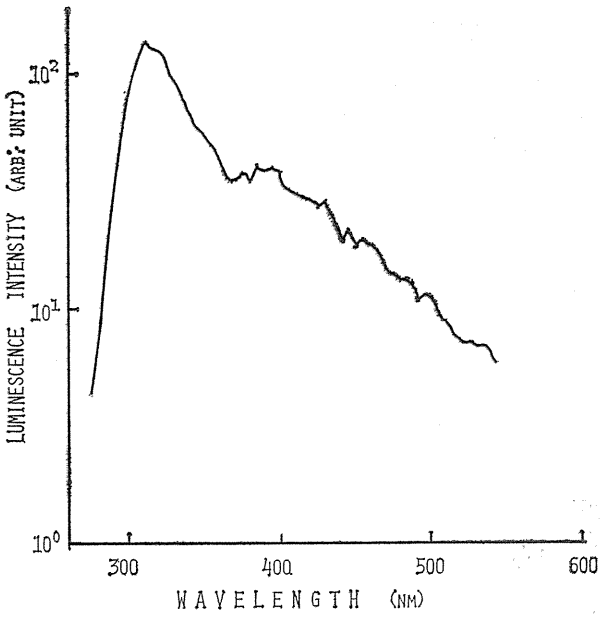

Fig. 14. Luminscence spectrum from PS.

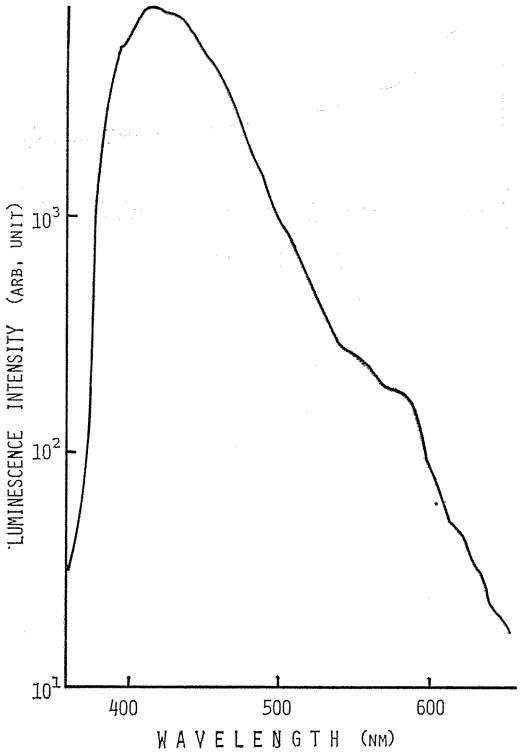

Fig. 15. Luminescence spectrum from PEN.

spectra are also shown. These phosphorescence could hardly be observed at room temperature, but at −185℃ their lifetime was expected to be longer than about 0.3 msec. The excitation spectra of both fluorescence and phosphorescence from PET, PPX and also PS (fluorescence) showed their maxima at around 310, 280 and 270 nm, which correspond to the wavelengths of the π π^* transition ($^1B_{2u} \longleftarrow {}^1A_{1g}$). Fluorescence study for PS, which revealed[22, 23] that excimer emission is observed around 330 nm, when measured on solid PS, shows similar results to the present results.

2) Photoconduction

The photocurrent in PET excited at 300 nm is shown in Fig. 16. On illuminating, the photocurrent abruptly increased and then gradually decreased even under illumination. The peak photocurrent and the steady state photocurrent are conveniently denoted by J_p and J_s, respectivly. The steady state photocurrent J_s is

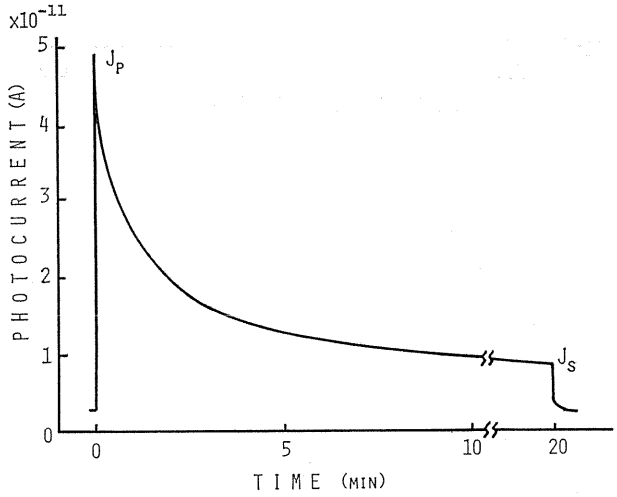

Fig. 16. Photocurrent response in PET (300 nm, -7.2×10^5 V/cm).

affected by space charges.

Photocurrent spectrum of PET corrected for light intensity obtained at a scanning rate of 34 nm/sec. is shown in Fig. 17. The photocurrent spectrum showed two peaks around 300 nm and 260 nm, which closely coincides with those of absorption spectrum. The optical energy for these π π^* excitations ($^1B_{2u} \longleftarrow {}^1A_{1g}$ and $^1B_{1u} \longleftarrow {}^1A_{1g}$) seems not enough to generate an electron-hole pair in PET. The absorbed energy seems to migrate as excitons, which will be at last dissociated to a free electron and a hole. Dissociation processes can be classified into a one photon process and a multi-photon process. These can be discriminated from a dependence of photocurrent on the light intensity.

As shown in Fig. 18, J_p depended linearly on the light intensity, suggesting a one photon carrier generation process. In Table 5, one photon dissociation processes of excitons are summarized. In polymers such as PET having rather low permittivity ($\varepsilon_r=3.0 \sim 3.2$), spontaneous ionization seems unexpective. In the case of

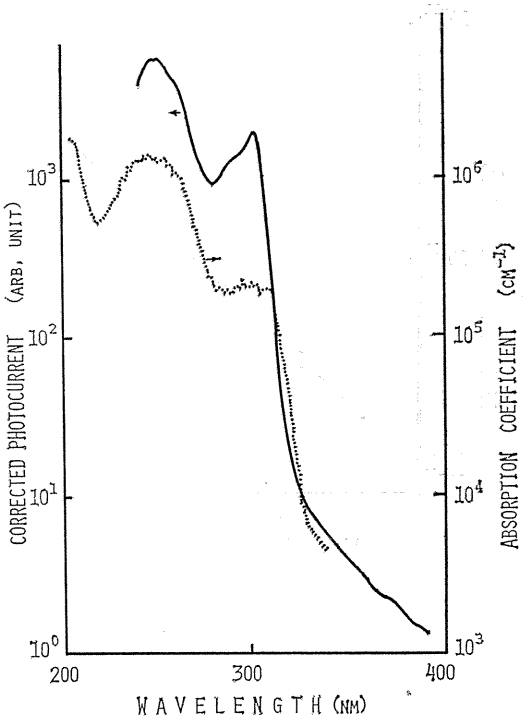

Fig. 17. Spectra of photocurrent and absorption coefficient in PET.

Table 5. Dissociation of excitons.

Dissociations of excitions by the one photon process
1. Spontaneous ionization of an exciton
2. Thermal ionization of an exciton
3. Field ionization of an exciton
4. Collision of an exciton with a dissociation center
5. Collision ionization of an exciton with surface
6. Liberation of a trapped carrier by an exciton

thermal dissociation, photocurrents should be thermally activated. The photocurrent in PET, however, scarcely depended on temperature as shown in Fig. 19 below the glass transition temperature. Field associated dissociation may be likely in this case. There are various fields in polymers, such as an applied field, surface potential and local fields around ionized impurities or trapped carriers. Since photocurrents can be observed even in the absence of any applied fields as mentioned later, externally applied fields seem not to play a dominant role in the carrier generation process. Surface potential is reported to be sufficient to ionize the exciton in PVK.[24] The interaction with charged defects (or traps) can also dissociate excitons as reported in anthracene crystals.[25] We have observed an enhancement of photoconductivity in PET by a previous γ-irradiation.[26] This suggests that the

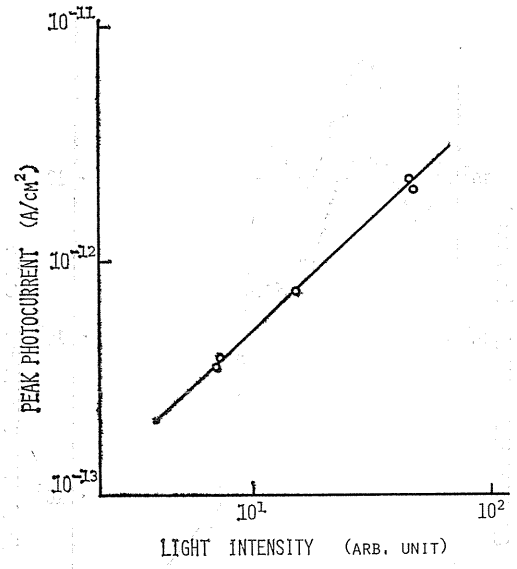

Fig. 18. Dependence of photocurrent in PET on the relative light intensity (-3.7×10^4 V/cm).

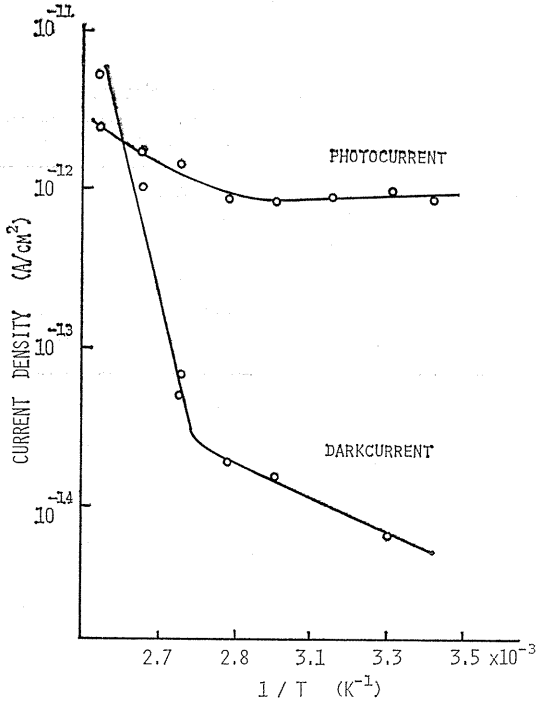

Fig. 19. Temperature dependence of peak photocurrents and dark currents in PET (300 nm, -3.7×10^4 V/cm, 10^{-3} Torr).

trapped carriers introduced by γ-irradiation may interact with excitons. The sign of dominant photocarriers can be determined as follows. The penetration depth is so small in the range shorter than 320 nm that excitation will occur near the illuminated surface. The diffusion of these spatially inhomogeneous photocarriers into bulk results in either sign of short-circuit photocurrents or open photovoltages depending on the kind of major carriers. The result is shown in Fig. 20 a), b), indicating that the dominant carrier is an electron in PET. This conclusion is supported by the polarity effect that photocurrents with a negative electrode illuminated are larger by more than one decade than that with a positive one illuminated.

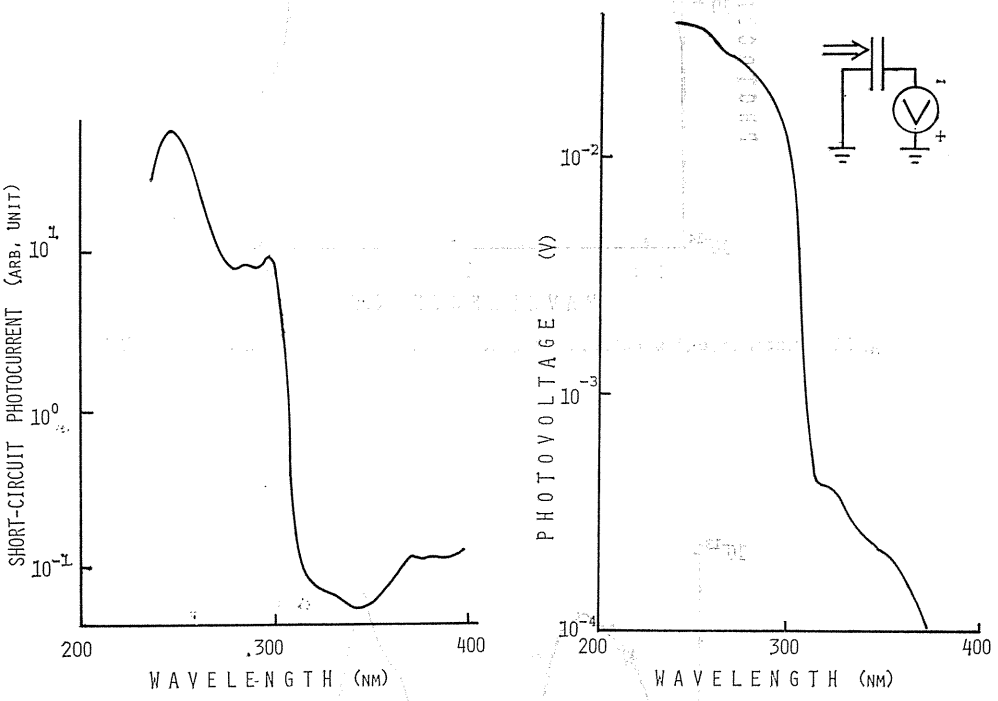

Fig. 20. a) Short-circuit photocurrent spectrum in PET.
b) Open photovoltage spectrum.

Photocurrent spectrum of PEN is shown in Fig. 21 (not corrected). The correspondence seems not so clear as compared with the case of PET. It seems appropriate for PEN to discuss the short-circuit photocurrent rather than that in the presence of applied fields as shown in Fig. 22. Peaks around 358 nm and 300 nm are considered to correspond to the peaks observed around 300 nm and 260 nm for PET. In the case of PEN, the allowed transition $^1E_{1u} \longleftarrow {}^1A_{1g}$ is so clearly shifted to 244 nm that the corresponding photocurrent can be well discussed. The former two peaks show a symbatic relation between the photocurrent and the absorption spectra, but the latter shows an antibatic relation. The antibatic relation can be understood from increased surface recombination resulting from the extremely high absorption coefficient, which is often observed in other materials[27] and also theoretically discussed.[28] The light intensity dependence of photocurrent

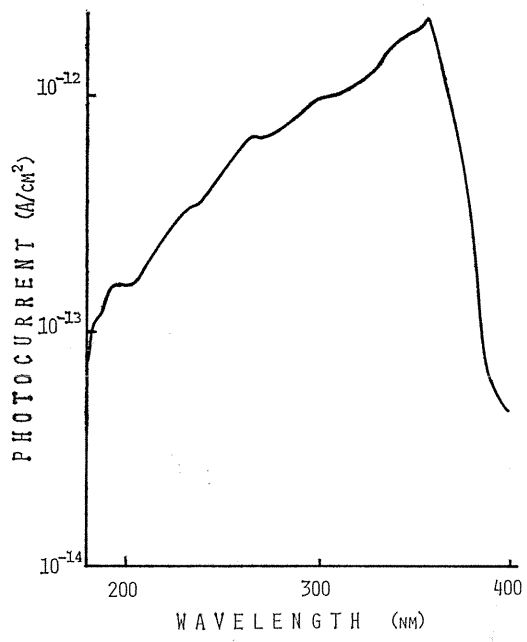

Fig. 21. Photocurrent spectrum (Au, 10^{-3} Torr, 4×10^{4} V/cm, 28℃) in PEN.

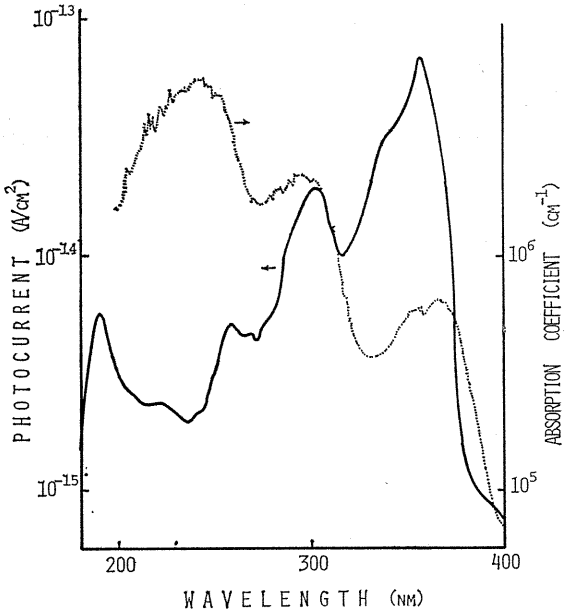

Fig. 22. Absorption coefficient and short-circuit photocurrent spectra.

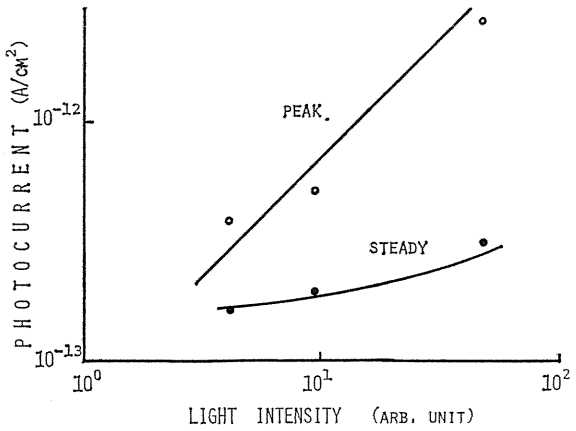

Fig. 23. Intensity dependence of photocurrent (3.2×10^5 V/cm, 10^{-3} Torr, 360 nm).

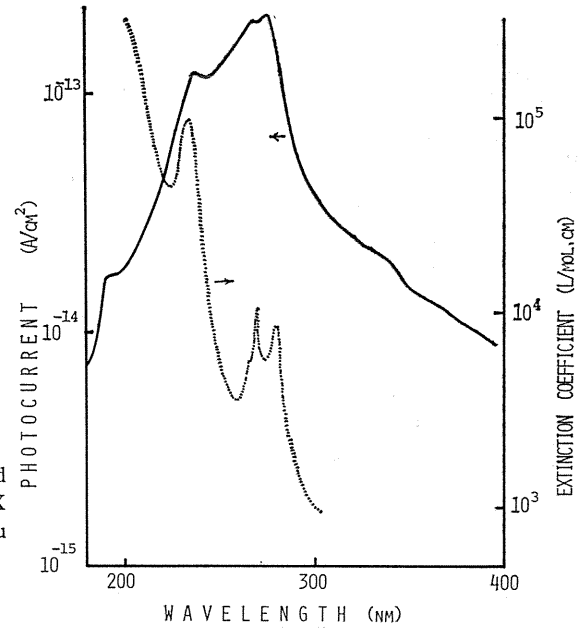

Fig. 24. Spectra of photocurrent and absorption coefficient in PPX (-3.7×10^4 V/cm, in N_2, Au electrode).

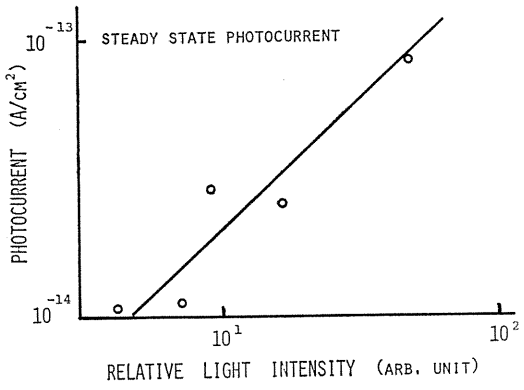

Fig. 25. Intensity dependence of steady state photocurrent in PPX (-3.7×10^4V/cm, 275nm, 10^{-3} Torr).

J_p for PEN is shown in Fig. 23, indicating a similar linear dependence to that of PET.

Photocurrent spectrum for PPX is shown in Fig. 24. A clear symbatic relation can be observed as in the case of PET. The photocurrent peaks at 275 nm and 225 nm correspond to the peaks at 300 nm and 260 nm for PET. Photocurrent at 275 nm shows a linear dependence on the light intensity as observed in Fig. 25. They show a somewhat different time dependence from that for PET, PEN, that is to say, the photocurrent in PPX showed not a sudden but only a slight decrease during illumination. This may suggest the photocurrent in PPX is not seriously affected by space charges.

For PS and PC, photocurrent spectra were obtained as shown in Fig. 26 a) and b), indicating a symbatic relation.

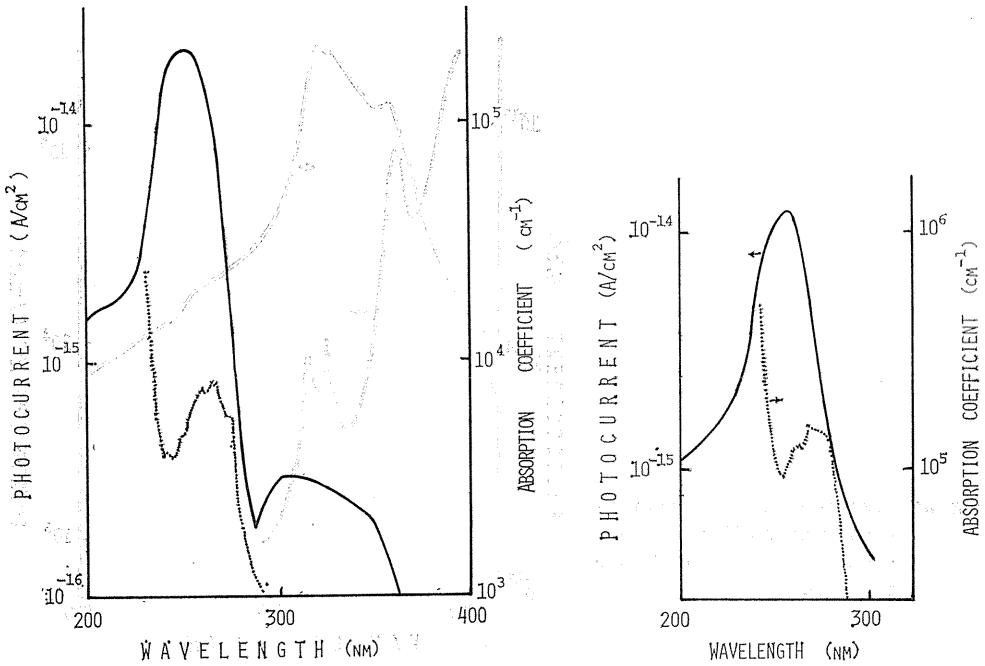

Fig. 26. a) Spectra of photocurrent and absorption coefficient in PS (-3×10^4V/cm, in N_2, UVD25).
b) Spectra of photocurrent and absorption coefficient in PC (-3.5×10^4V/cm, in air, UVD25).

From these similar behaviors to that of PET, photocarriers are supposed to be generated through a certain one photon dissociation process of excitons in the case of PEN and PPX. The sign of dominant photocarriers is concluded to be electrons in all these polymers from similar experiments mentioned above.

3. 2. 3. Photocarrier Injection from Electrodes

It has been suggested by several investigators[29)~31)] that the photoconduction in polymers is induced by carrier injection from electrodes. The photoinjection

phenomena may be predominant especially in the wavelength range of small optical absorption.

1) Photocarrier Injection Spectra

Photocurrent spectra in PET with four electrode materials (Al, Cu, Ag, Au) are shown in Fig. 27. Semitransparent Au electrode was used as the illuminated electrode commonly for each specimen, otherwise the light intensity at the boundary between metal and PET should not be consistent among these various metals because of the difference of their transparencies. The photocurrent in the range longer than 320 nm seriously depended on the electrode material, but was hardly affected in the range shorter than 320 nm, because the carrier generation through excitons shown in § 3. 2. 2 was more dominant than the injection. Figure 28 shows the

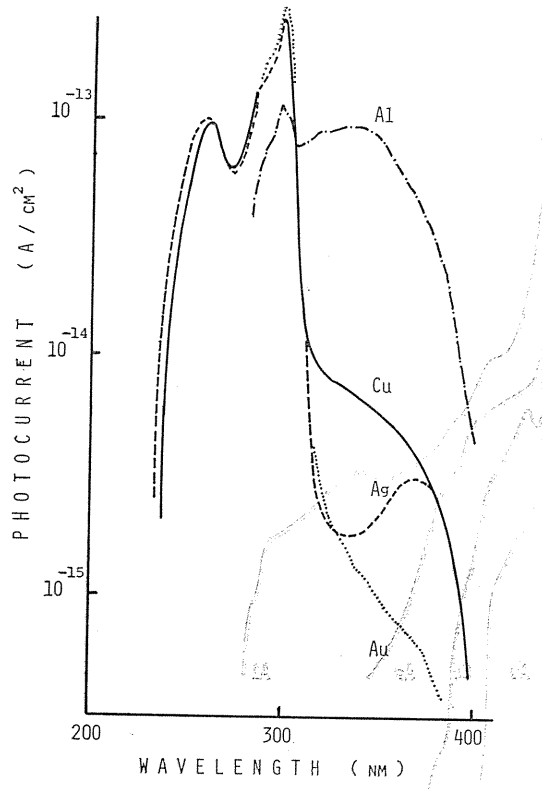

Fig. 27. Electrode effects on photocurrents in PET (-3.7×10^4 V/cm, in air).

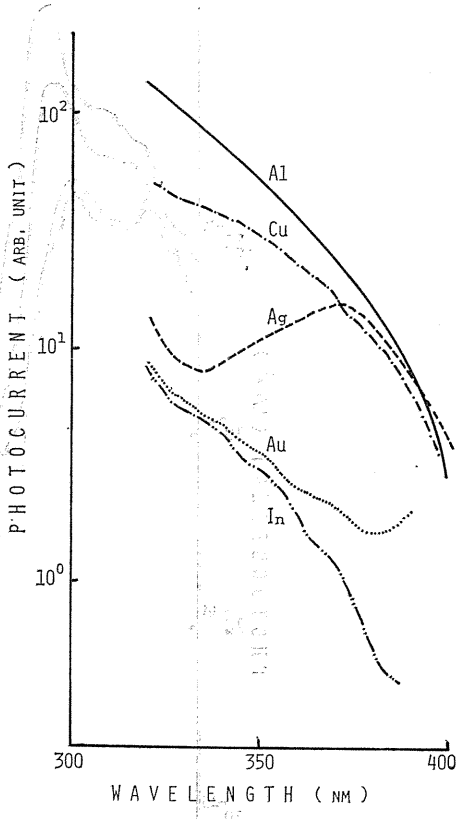

Fig. 28. Spectra of photoinjection currents corrected for the light intensity.

corrected photoinjection currents as a function of wavelength. The electric field was applied in such a direction that the electrons injected from the bottom various metal electrodes were drifted towards the upper illuminated electrodes. In the case of Al, Cu, Ag at least, the photoinjection from electrodes plays a dominant part in the photocurrent in the wavelength range longer than 320 nm.

Similar results were obtained for the other polymers. Thep hotoinjection spec-

tra are shown in Figs. 29 ~ 34 for PEN, PPX, PS, PC, PE and PVC, respectively. Generally, similar tendency to the case of PET can be observed, that is to say, Au electrode can scarcely inject carriers but Al electrode can easily inject. The spectra for PEN show the duplicate photoconduction process of the exciton induced photoconduction and photoinjection from metal electrodes of Al and Ag in the region shorter than 400 nm. For PPX, a minimum of the photoinjection current was observed around 340 nm, which is similar to that of PET. Photoinjection currents into both PC and PS were large enough to overwhelm the exciton induced photocurrent which was fairly small as compared with PET, PPX and PEN. In the saturated polymers of PE and PVC, photocurrents were affected also by the injection especially from Al.

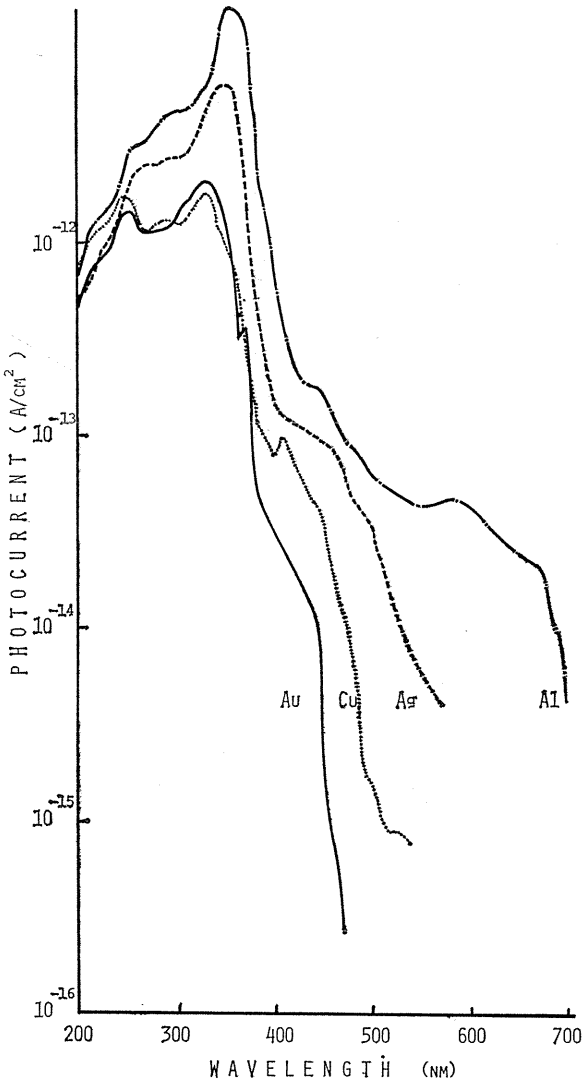

Fig. 29. Electrode effects on photocurrents in PEN (4×10^4 V/cm).

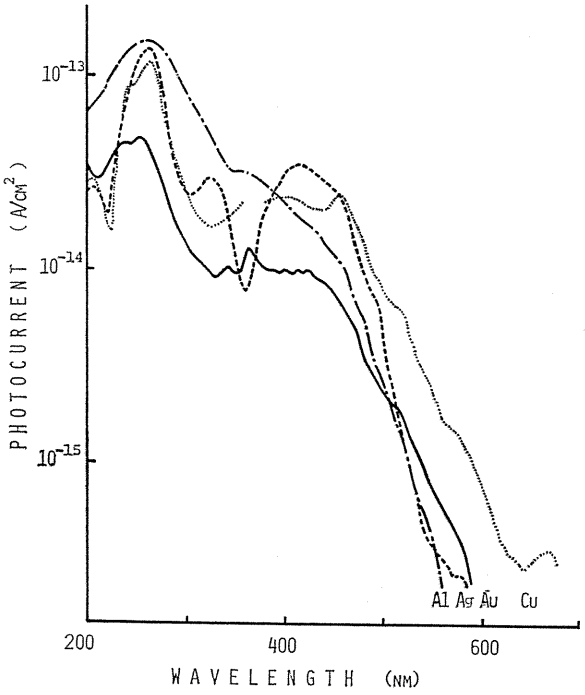

Fig. 30. Electrode effects on photocurrents in PPX (2×10^4 V/cm).

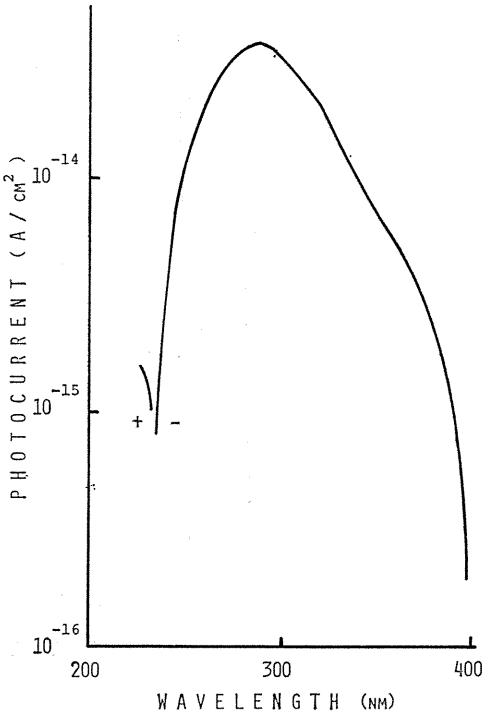

Fig. 31. Photoelectron injection current spectrum from Al into PS (-3×10^4 V/cm, in N_2, UVD25).

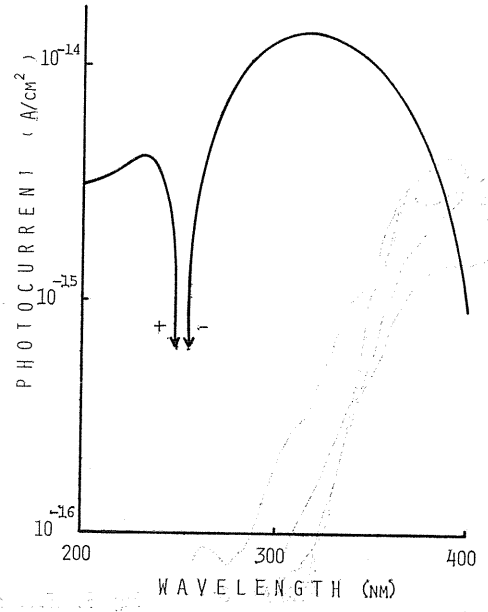

Fig. 32. Photoelectron injection current spectrum from Al into PC (-1.8×10^4 V/cm, in N_2, UVD25).

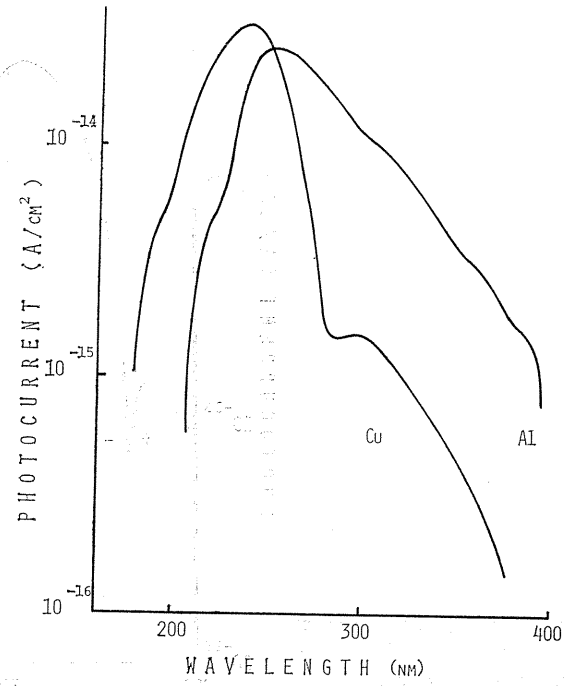

Fig. 33. Photoelectron injection current spectrum from Au and Cu into LD-PE (4.5×10^4 V/cm, 10^{-3} Torr).

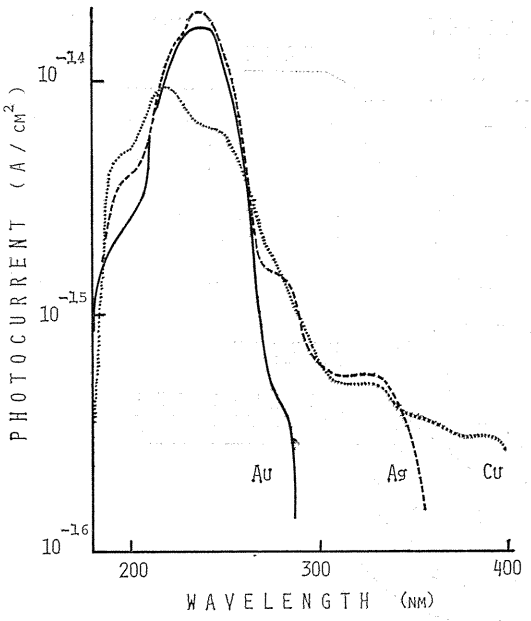

Fig. 34. Photoelectron injection current spectrum from Al, Ag and Al into PVC (-4.5×10^4 V/cm, 10^{-3} Torr).

2) Sign of Injected Carriers

Several methods have been proposed to determine the sign of injected carriers for semiconductors, but for polymers, they showed unsuccessful results[32] because of the low mobility and/or the small carrier density. Only a few methods can be available for polymers. The polarity effect may be able to show which sign of carriers are injected. In such experiments, however, conventional sandwich type electrode configuration is commonly used, in which both electrodes are illuminated by light scarcely absorbed by the specimen, so that the carrier injection should take place at both electrodes, which leads to the obscure decision. The systematic study of the correlation between the metal workfunction and the photocurrent threshold energy seems to be also able to decide the sign, but there are not necessarily direct correlations between them on account of some factors controlling the carrier injection phenomena, such as surface states. Consequently, this method is not always a decisive one for the determination of the sign of injected carriers. Avoiding these imperfections, we have developed a new experimental technique, by which the sign of carriers injected from the illuminated electrode into polymers can be determined from the sign of photoinjection currents. This was conducted for PET using a particular electrode configuration shown in Fig. 35. In spite of the sandwich type electrode configuration, the only one electrode can be illuminated from which carriers are injected and diffuse towards the unilluminated (carefully masked) collecting electrode under short-circuit condition. The direction of this diffusive photocurrent will show the sign of the injected carriers. A typical result for Al is shown in Fig. 36. The direction of the photocurrent indicated that electrons were injected. For the case of Cu electrode, the short-circuit photocurrent was

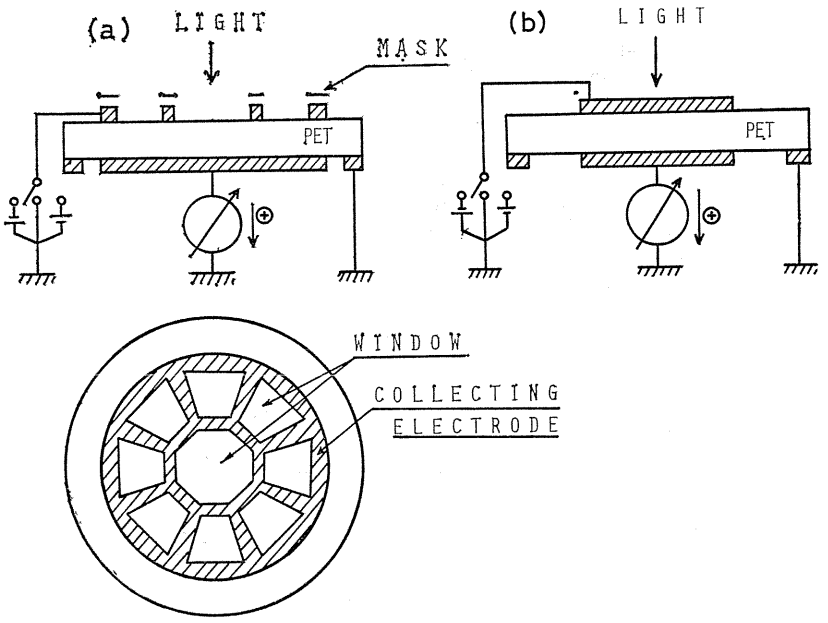

Fig. 35. A new electrode configuration to determine the sign of the injected carriers (a) and a conventional type electrode (b).

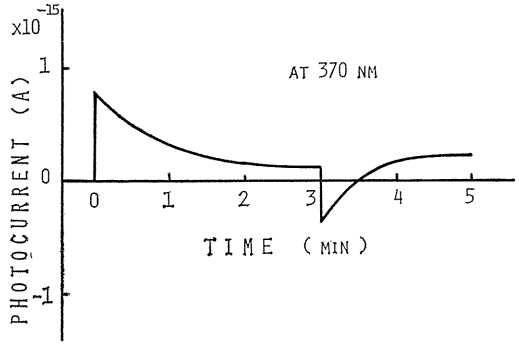

Fig. 36. Photocurrent response with Al electrode [type (a)].

too small to discuss, so a small collecting field was applied. The result is shown in Fig. 37. When Cu electrode was in the positive polarity, the signal could scarcely be observed, while in the negative polarity, it was large enough to conclude the injected carriers to be electrons. The other metal electrodes showed so small signals even with a collecting voltage that we employed the conventional sandwich type electrode configuration with Au colllecting electrode which was found to show an extremely small signal in the above experiments. For Ag electrode, a minimum of photoinjection current was observed around 340 nm in Fig. 27. The short-circuit photocurrents at 340 nm and 370 nm are shown in Fig. 38, suggesting hole injection and electron injection to become dominant around 340 nm and 370 nm, respectively.

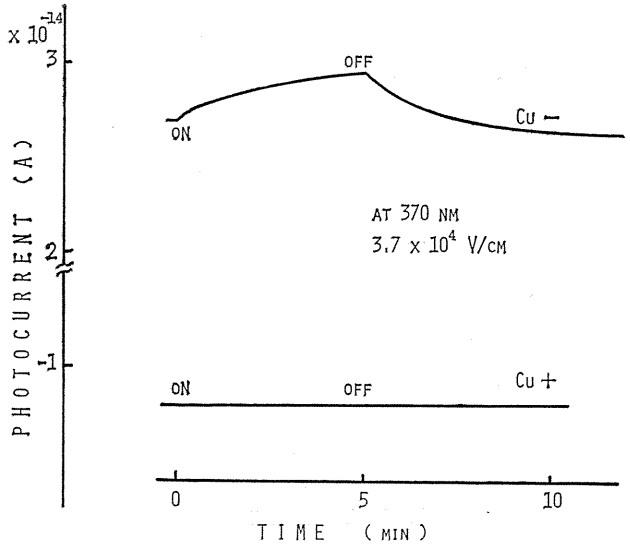

Fig. 37. Polarity effect of photocurrents with Cu electrode [type (a)].

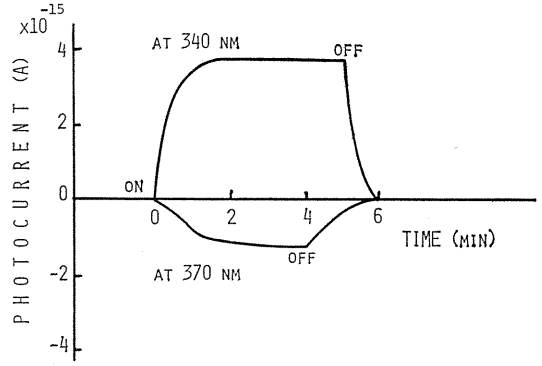

Fig. 38. Short-circuit photocurrent with Ag electrode [type (b)].

This suggestion is also supported by the polarity effect shown in Fig. 39. When a positive field was applied to the Ag electrode the photocurrent around 370 nm was suppressed and showed no peak, but increased around 340 nm as compared with the negatively applied case. For Au and In electrodes, dominant injected carriers could not be determined. In these extremely low injection cases, it may be possible for the photocurrent to be due to impurity excitation. It is, however, hard to discuss further because of the infinitely small magnitude of photocurrents.

The injected carriers into other polymers are also considered to be mainly electrons for Al, Cu by an analogy of the result of PET. For PPX, a possibility of hole injection from Ag is also suggested from the result of Fig. 30.

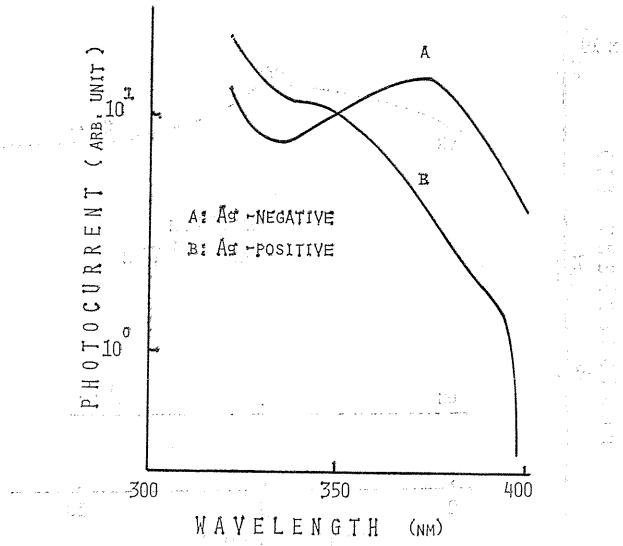

Fig. 39. Polarity effect of photocurrents with Ag electrode [type (b)].

3) Barrier Height and Surface States

Barrier height and surface states of metal-insulator contacts have scarcely been discussed. Davies[33] has reported that the contact charging of insulating polymers is caused by the electron injection to or from the polymer bulk, while Bauser et al.[34] and Krupp[35] have suggested that the contact charging is induced by the electron transfer from surface states.

The contact barrier heights for PE and PET were recently reported[36] as 2.14 eV and 2.58 eV, respectivvely, which were estimated from the experimental result of Schottky emission from metal electrodes (Al).

As mentioned above, photocurrents in PET witth Al and Cu elctrodes are considered to be induced by the photoelectron injection from electrodes in the range of 400 ~ 320 nm. The threshold energy for the photoinjection current can give directly the barrier height of a metal-polymer contact.

For a given photon flux, the photoinjection current J is expressed to a first approximation by[37]

$$J=AT^2f(x), \tag{1}$$

where $x=(h\nu-\phi_c)/kT$, A is a constant, k is Boltzman's constant, T is the absolute temperature, $h\nu$ is the incident photon energy, ϕ_c is the threshold energy, and

$$f(x)=e^x-\frac{e^{2x}}{4}+\frac{e^{3x}}{9}-\cdots \qquad x<0 \tag{2}$$

$$f(x)=\frac{\pi^2}{6}+\frac{x^2}{2}-\left(e^{-x}-\frac{e^{-2x}}{4}+\frac{e^{-3x}}{9}-\cdots\right) \qquad x>0. \tag{3}$$

For large x ($x>4$), $f(x)$ can be approximately expressed by

$$f(x)\simeq\frac{x^2}{2}, \tag{4}$$

then, the photoinjection current J reduces to the familiar Fowler's equation,

$$J\propto(h\nu-\phi_c)^2. \tag{5}$$

Thus, the plot of the square root of J versus $h\nu$ gives a straight line. An intersection of the straight line with the $h\nu$ axis will give a threshold energy ϕ_c which is the barrier height of a metal-polymer contact.

Photoinjection currents obtained in vacuum for Al and Cu electrodes are plotted as the square root of photocurrent against photon energy (*i. e.* the Fowler plot) in Fig. 40. The results show the barrier heights for Al and Cu to be 2.83 and 2.90 eV, respectively. The value of 2.83 eV well agrees with 2.58 eV obtained from

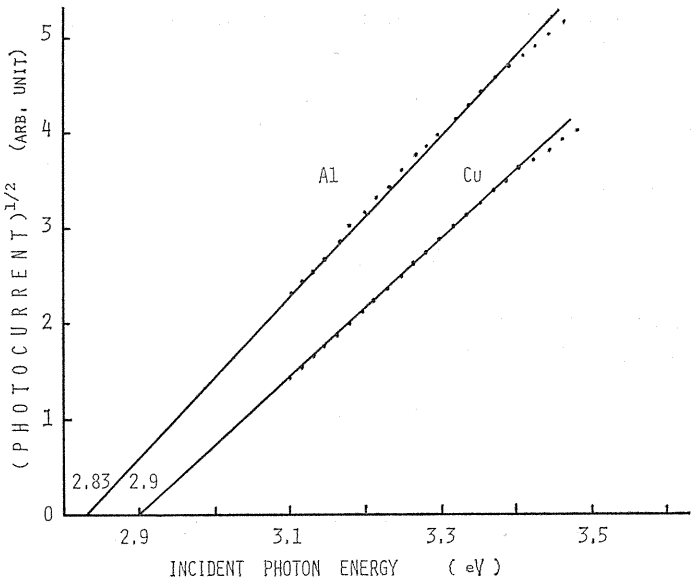

Fig. 40. Fowler plot of the photoinjection current in PET.

the result of Schottky emission.[36] The workfunction of Al and Cu was evaluated from the external photoemission experiment to be 3.44 eV and 4.54 eV, respectively. The difference in the barrier height between actual Al-PET and Cu PET contacts is only 0.01 eV, while it should be 1.1 eV if the surface states have not been present. This suggests the presence of a high density of surface states on the PET surface.

When the surface states are taken into account, the contact phenomena can be considered as follows. We considered an insulator with uniformly distributed surface states whose density is N_s states cm^{-2} eV^{-1} in the forbidden gap. Before contact, the surface states will be filled to an energy ϕ_{co} below the bottom of the conduction band as shown in Fig. 41 a). If the workfunction of the metal electrode ϕ_m is, for example, smaller than that of the insulator surface ϕ_{is}, electrons are

transferred from the electrode into the surface states during contact. The difference in potential $\phi_{is}-\phi_m$ can be reduced in the doubly charged surface layer

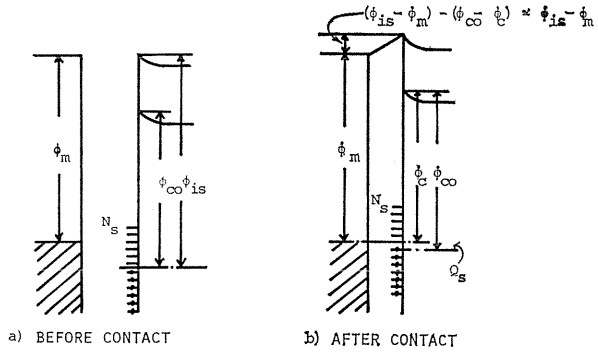

Fig. 41. Model for the polymer-electrode contact with surface states

without appreciably altering the potential barrier at the insulator surface if the density of surface states is sufficiently high (Fig. 41 b)). If we assume that the surface states are filled to an energy ϕ_c below the conduction band, the electronic charge transferred per unit area (Q_s) is expressed as

$$Q_s=qN_s\frac{\phi_{co}-\phi_c}{q}, \tag{6}$$

where q is charge of an electron. We can consider that the potential across the contact surface layer is given by

$$q\Delta V=(\phi_{is}-\phi_m)-(\phi_{co}-\phi_c), \tag{7}$$

and we obtain

$$Q_s=C_s\Delta V=\frac{\varepsilon_i\varepsilon_o}{qs}[(\phi_{is}-\phi_m)-(\phi_{co}-\phi_c)], \tag{8}$$

where, C_s is the capacitance per unit area of the interfacial layer, ε_i is the dielectric constant of the interfacial layer and s is its thickness. From equations (6) and (8),

$$N_s(\phi_{co}-\phi_c)=\frac{\varepsilon_i\varepsilon_o}{qs}[(\phi_{is}-\phi_m)-(\phi_{co}-\phi_c)]. \tag{9}$$

If the values of the threshold for photoinjection ϕ_{c1} and ϕ_{c2} are obtained for two different matals whose workfunctions ϕ_{m1} and ϕ_{m2} are already known, we can estimate the density of surface states N_s as

$$N_s=\frac{\varepsilon_i\varepsilon_o}{qs}\frac{(\phi_{m1}-\phi_{m2})-(\phi_{c1}-\phi_{c2})}{\phi_{c1}-\phi_{c2}} \tag{10}$$

$$=\frac{\varepsilon_i\varepsilon_o}{qs}\frac{\phi_{m1}-\phi_{m2}}{\phi_{c1}-\phi_{c2}} \quad \text{if} \quad \phi_{m1}-\phi_{m2}\gg\phi_{c1}-\phi_{c2}. \tag{11}$$

The thickness of the interfacial layer s is of the order of interatomic spacing and the dielectric constant ε_i of such a thin layer can be approximated by the free space value.[38] If we assume that $s=5$ Å and $\varepsilon_i=1$, we obtain for Al and Cu into equation (11).

Atmospheric effects on the photoinjection current from Cu into PET were investigated in the presence of various gases, namely, helium, nitrogen and oxygen as well as in vacuum. The result is shown in Fig. 42, which demonstrates a strong dependence of the photocurrent on the atmospheric conditions. Threshold energies for

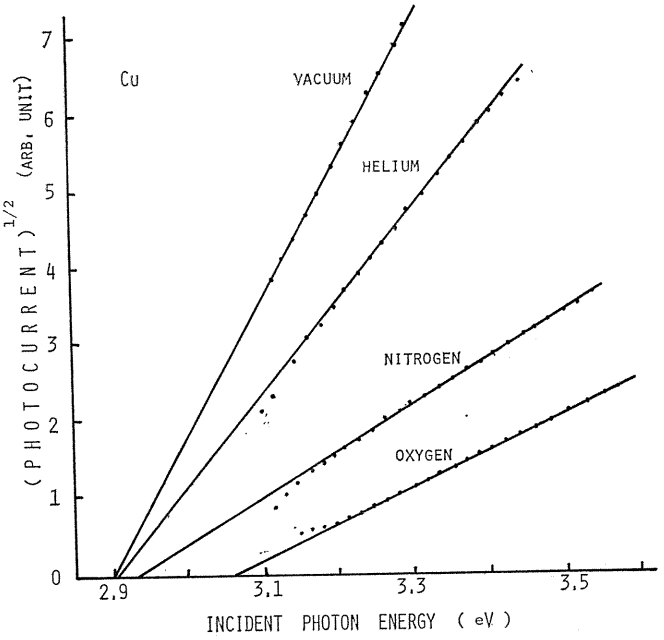

Fig. 42. Fowler plot of the photoinjection current from Cu in various gases.

Cu-PET contact were 2.90 eV in vacuum, 2.91 eV in He, 2.94 eV in N_2 and 3.06 eV in O_2. Oxygen caused an extreme increase in the contact barrier height as compared with the other gases. The O_2 molecules absorbed on PET surface can trap electrons because of their high electron affinity and act as additional surface states as schematically shown in Fig. 43. When the barrier height ϕ_c(vac) (in vacuum) increases to $\phi_c(O_2)$ by introducing O_2 gas, the increase in the surface charge is given by

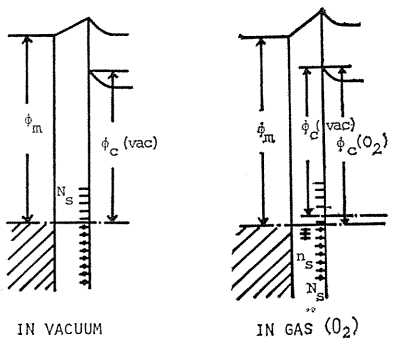

Fig. 43. Effects of O_2 gas on the contact.

$$Q_s=\frac{\varepsilon_i\varepsilon_o}{qs}[\phi(O_2)-\phi_c(\mathrm{vac})]. \tag{12}$$

If we assume that the density N_s of the surface states is independent of the absorbed O_2 molecules, the number of charged surface states originating from absorbed O_2 molecules, n_s (O_2) is given by

$$n_s(O_2)=\frac{\varepsilon_i\varepsilon_o}{q^2s}[\phi_c(O_2)-\phi_c(\mathrm{vac})]+\frac{N_s}{q}[\phi_c(O_2)-\phi_c(\mathrm{vac})]. \tag{13}$$

When we use ϕ_c $(O_2)=3.06$ eV, ϕ_c (vac) $=2.90$ eV and $N_s=1.7\times10^{14}$ cm^{-2} eV,$^{-1}$ we obtain

$$n_s(O_2)=2.9\times10^{13} \quad \text{states cm}^{-2}. \tag{14}$$

Similar photoinjection currents were observed in PE. In the case of, PE, the photoinjection current was considerably small as compared with the case of PET as shown in Fig. 33 (obtained using monochromatic light). Consequently, the contact barrier height was not exactly estimated, but the result obtained from the experiment with colored glass filters showed the threshold energies to be in the range of $2.7 \sim 3.5$ eV for Al and $2.5 \sim 2.7$ eV for Mg as obserbed in Fig. 44. The photoinjection current from Al into PE showed an anomalous transient behavior as

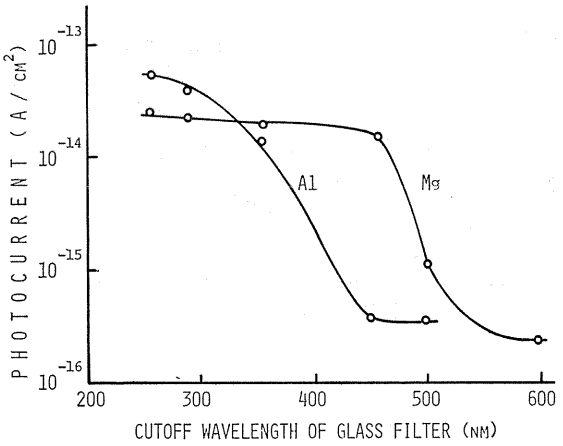

Fig. 44. Photoinjection currents from Al and Mg into LD-PE.

indicated in Fig. 45. A transient short-circuit photocurrent flew in the direction that injected electrons from Al diffused towards a collecting Au electrode. A similar transient, but opposite polarity, followed on removal of light (white light from xenon lamp). The "on" transient photocurrent had a simple time constant τ as shown in Fig. 46, over the temperature range of $-140 \sim 100$℃. Figure 47 shows a dependence of the time constant τ on the reciprocal temperature, which indicates that the decay time constant τ can be expressed by

$$\tau=\tau_0\exp(U/kT), \tag{15}$$

where τ_0 is a constant and U is the activation energy estimated at about 0.1 eV from the slope of the straight line in Fig. 47.

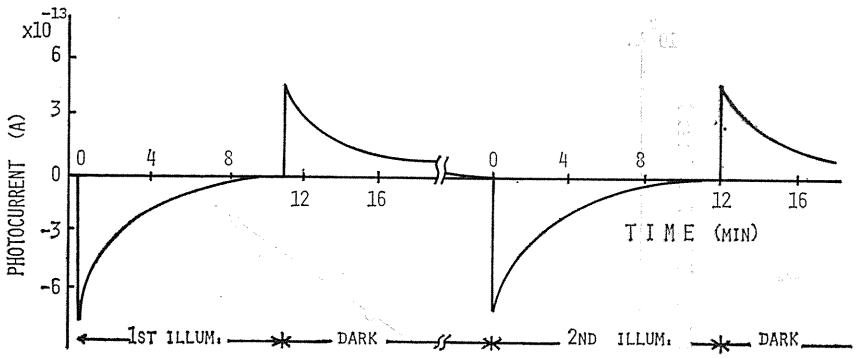

Fig. 45. Photocurrent response in LD-PE with Al electrode when illuminated with white light from xenon lamp at 0 V/cm.

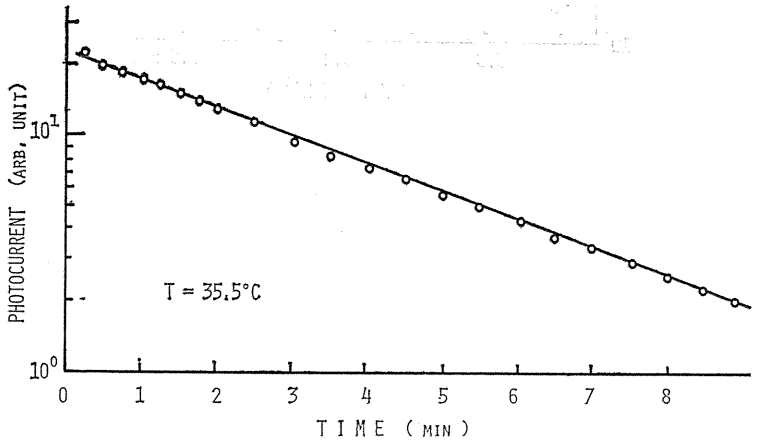

Fig. 46. Decay of photoinjection current from Al into LD-PE.

A possible mechanism of this phototransient current with Al electrode may be as follows. On illumination, electrons are injected from Al electrode into the polymer-electrode interface and most of them are trapped near the interface without diffusing deeply into the bulk because the time constant was rather short and the hysteresis effect was not so prominent. At the same time, these electrons trapped are thermally released from the trap and return to the Al electrode under the influence of the image charge field. As the number of trapped electrons near the interface grows with time, the electron released from traps and returning to the electrode increases till an equilibrium is attained between the injection and the reverse current to the electrode. On removal of illumination, the photoinjection of electrons ceases and only the current due to the electrons which return to the electrode is observed. Thus, the direction of the "off" transient current shows an opposite direction to the "on" transient photoionjection current.

Assuming a single set of traps at E_t and the avarage penetration depth l of injected electrons and a slow retrapping where released electrons from traps return to the electrode before retrapping, we obtain

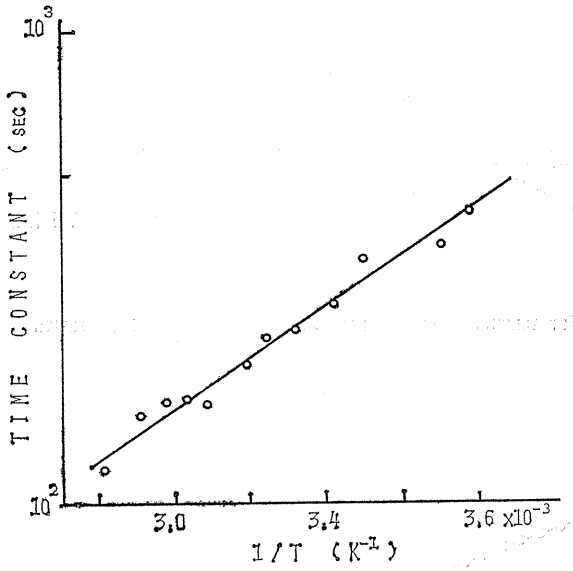

Fig. 47. Temperature dependence of the decay time constant τ of the photoinjection current from Al into LD-PE.

$$J(t) = -|q|\frac{l}{d}\frac{\mathrm{d}n(t)}{\mathrm{d}t}, \tag{16}$$

$$\frac{\mathrm{d}n(t)}{\mathrm{d}t} = f\alpha - \frac{n(t)}{\tau}, \tag{17}$$

where, $J(t)$ is the observed current density, d is the distance between two electrodes, $n(t)$ is the surface density of electrons trapped at the electrode-polymer interface, f is the light intensity, α is the number of injected electrons / cm^2 per unit light intensity per second and τ is the lifetime in traps of the depth E_t expressed by

$$\tau = \tau_0 \exp\left(\frac{E_t}{kT}\right). \tag{18}$$

Equations (16) and (17) can be easily solved in each case of "on" and "off" transient currents. For "on" photocurrent, we obtain

$$J(t) = -|q|f\alpha\frac{l}{d}\exp\left(-\frac{t}{\tau}\right), \tag{19}$$

assuming the initial condition $n\ (0)=0$. For the "off" transient current, we obtain,

$$J(t) = |q|f\alpha\frac{t}{d}\exp\left(-\frac{t-t_0}{\tau}\right), \tag{20}$$

assuming $n(t_0)=f\alpha\tau$, where t_0 is the time when light is turned off.

Equations (19) and (20) show an exponential decay with time constant τ, which

well explains the experimental results (Figs, 45 and 46). From equation (18), E_t can be evaluated. The result shown in Fig. 47 indicates the trap depth E_t to be 0.1 eV.

3. 2. 4. Optical Release of Trapped Carriers

Carrier trapping phenomena have been intensively investigated. Experimental techniques such as thermally stimulated current (TSC) and thermoluminescence(TL) have been applied to give many useful results, but they have some disadvantages arising from their nonisothermal properties. The TSC analysis assumes trapping parameters such as a trap depth and a capture cross section to be independent of temperature. It seems, however, unlikely in polymers, especially around characteristic temperatures at which melting or other molecular relaxations such as a micro-Brownian motion occurs. On the other hand, the photo-stimulated detrapping current (PSDC) analysis is an isothermal analysis, which can directly show an energetic distribution of traps at a given temperature. The discrimination between electronic and ionic traps is not easy in the TSC analysis, whereas only electronic carriers contribute to PSDC. The analysis of PSDC can evaluate extremely deep traps at a few eV, which can not be observed in TSC because of the low melting point of usual polymers.

1) PSDC Spectra

Figure 48 shows the effects of γ-ray (Co^{60}) irradiation and re-irradiation after annealing on the photocurrent in high density polyethylene (HD-PE). Curves A and

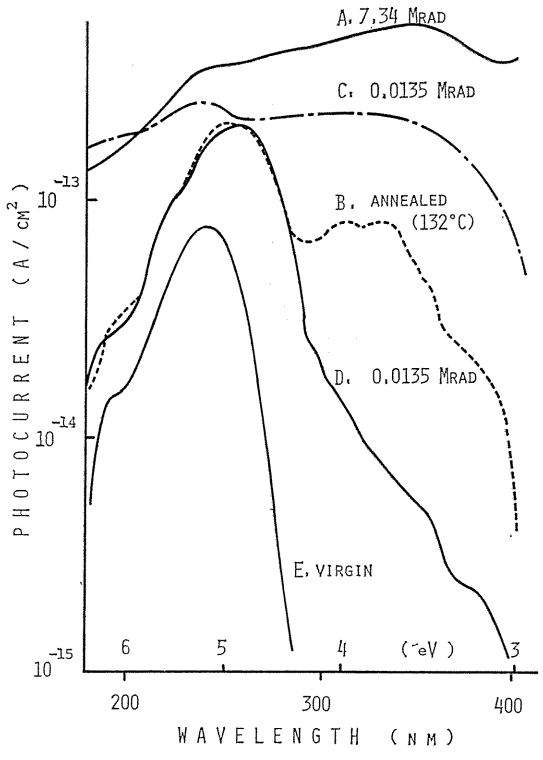

Fig. 48. Effects of γ-irradiation on the photocurrent in HD-PE and the effect of re-irradiation after annealing.

E are photocurrents in HD-PE after and before γ-irradiation of 7.34 Mrad (irradiated in $\sim 10^{-3}$ Torr). An extreme enhancement by γ-irradiation can be observed especially in the range of $3 \sim 4$ eV. Curve B is the result after annealing at 132℃ for 1 hour. The re-irradiation of an extremely small dosage (0.0135 Mrad) enhanced the photocurrent spectrum to curve C. On the other hand, γ-irradiation with the same small dosage (0.0135 Mrad) could only slightly increase the photocurrent for the specimen not previously γ-irradiated (curve D). These results indicate that the photocurrent in the range of $3 \sim 4$ eV is induced by the optical release of carriers captured by fairly deep traps introduced by γ-irradiation of 7.34 Mrad and that most of the deep traps survive even after annealing near the melting temperature. Crystallinity effect on the PSDC spectra is shown in Fig. 49, which indicates the results obtained for HD-PE, low density polyethylene (LD-PE)

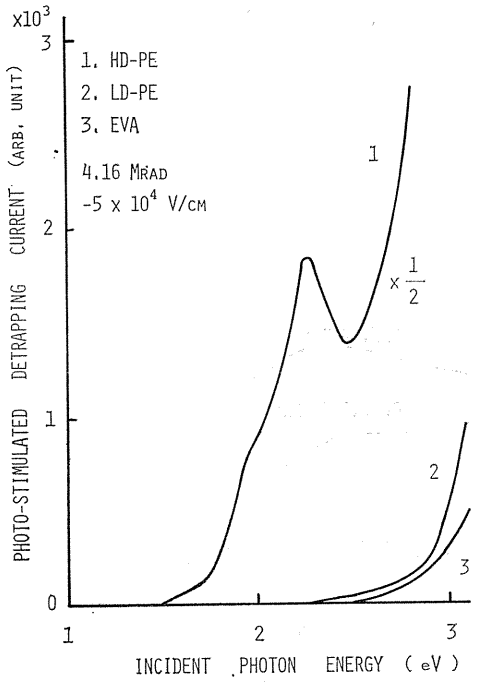

Fig. 49. Crystallinity effect on PSDC from LD-PE and EVA, irradiated in 10^{-3} Torr.

and ethylene-vinyl acetate copolymer (EVA), whose crystallinities are estimated at 75, 50 and 18%, respectively. The deep traps responsible for the photocurrent are intimately concerned with the crystallinity of the specimen. The larger the crystallinity, the larger the PSDC.

The PSDC from HD-PE irradiated in vacuum was greater than that in air by more than 50-fold as shown in Fig. 50 a). On the other hand, the photocurrent in LD-PE was rather complicated as shown in Fig. 50 b). LD-PE γ-irradiated in vacuum showed that two or three times larger photocurrent at the energy above 3.4 eV than that of LD-PE irradiated in air. On the other hand, the latter was

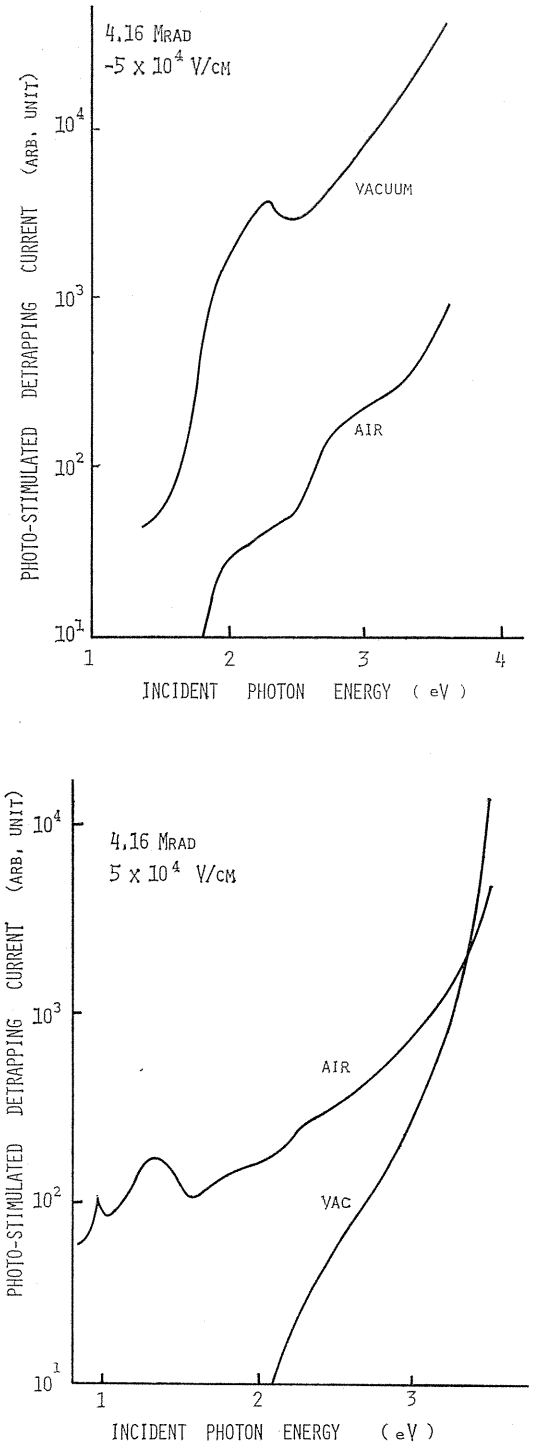

Fig. 50 a) Effect of atmospheric conditions during γ-irradiation for HD-PE.
b) Effect of atmospheric conditions during γ-irradiation for LD-PE.

greater than the former below 3.4 eV and showed a new remarkable peak around 1.3 eV. Different absorved dose was found to give similar results up to several 10 Mrad.

There have been many proposals as for the origin of traps, for example, O_2[39], oxidation products[40], unsaturation bonds[41, 42] and a methylene group[43], etc. In addition to these chemical traps, some physical traps are also reported such as the boundary[41] between the crystalline and the amorphous part, folded region of main chains[44] and cavities.[45]

Several defects introduced by γ-irradiation[46] could also act as a trap center. Three kinds of free radicals are generated in PE by γ-irradiation. Alkyl radicals are stable only at low temperature and almost disappear at room temperature. Allyl radicals scarcely decay at room temperature, but entirely disappear by heating above the melting point.[47] Polyenyl radicals can be relatively stable even at 150℃, but can be produced only at high dosage of 3×10^9 rad. Then the result of Fig. 48 excludes the possibility of free radical traps.

A scission of main chains occurs in PE together with crosslinking. Although the irregularity induced by the chain scission might be able to trap carriers, this is rejected by the following fact. The chain scission is more prominent in PE irradiated in air than that in vaccum.[48] This fact is contradictory to the results shown in Figs. 50 a) and b) showing a large PSDC in PE irradiated in vacuum than that in air (above 3.4 eV for LD-PE).

Defects such as crosslinks and double bonds (tr-vinylene) are more prominent in PE irradiated in vacuum than in air, because molecular oxygen interrupts the formation of crosslinks and double bonds.[49] These irregularities are considered to form the cavity trap. The apparent dependence of PSDC on the crystallinity shows that only the defects within or on the surface of the crystalline part can act as the deep trap. This is because defects in the amorphous part which has naturally no structual regularity are supposed to be unable to act as a deep cavity-like trap or only to act as a shallower trap if they could form traps.

In order to decide which of these defects was an origin of the deep trap, further exp eriments were carried eut. The G value of crosslinks increases with temperature above the glass transition temperature T_g, but it is independent of temperature for tr-vinylene unsaturations.[50] Eor the specimen irradiated with an electron beam, similar results to those by γ-irradiation should be obtained, because crosslinking and unsaturation bond formations are considered to be independent of a dose rate. On account of experimental requirement, a short time irradiation with high dose of an electron beam was conducted. Results are shown in Fig. 51, which were obtained by irradiating at room temperature and at higher temperature (85 ~ 65℃). The significant dependence of PSDC on irradiation temperature leads to the conclusion that the origin of the deep trap is mainly crosslinks, but not unsaturation bonds.

The result shown in Fig. 52 supports the above assignment. The γ-irradiation affected the photocurrent very slightly in PP which is known as a polymer with a small G value for crosslinking, *i. e.* 0.15[51], while 1.7[50] for PE.

These results together with the crystallinity effect suggest that the deep trap is associated with crosslinks in the crystalline part and/or in the interfacial region[52] between the crystalline and the amorphous part.

Figure 53 shows a temperature dependence of PSDC in γ-irradiated HD-PE. A

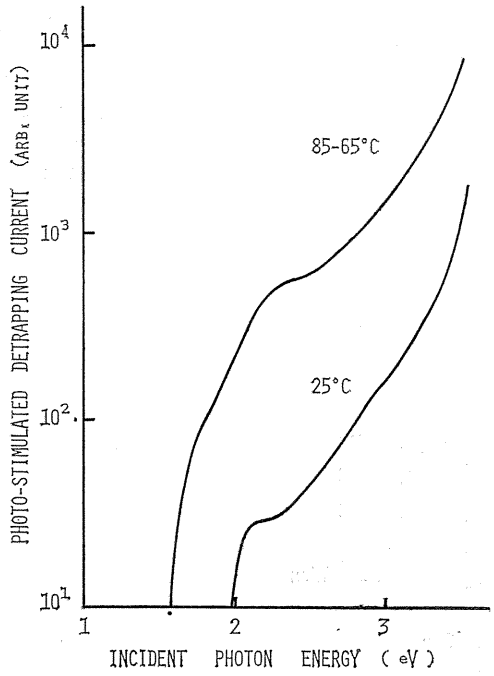

Fig. 51. Effect of irradiation temperature on PSDC in HD-PE. The result was obtained for electron beam irradiated PE in 10^{-3} Torr.

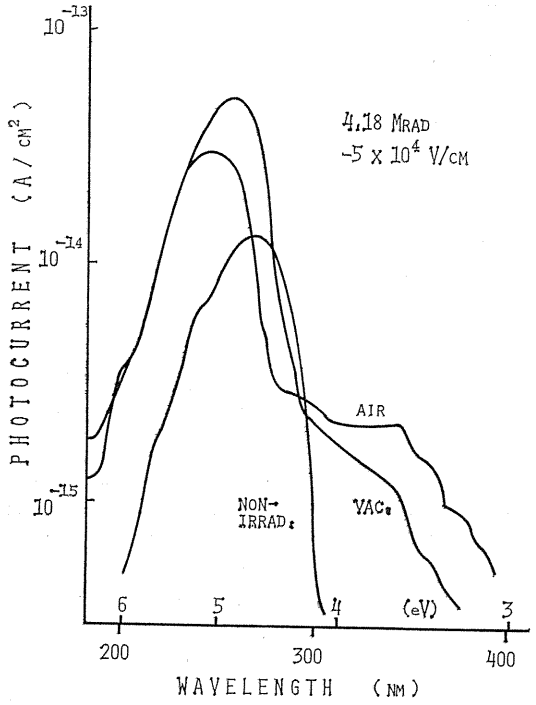

Fig. 52. PSDC spectra in PP γ-irradiated in air and in vacuum.

PSDC peak energy corresponding to the trap depth decreased with temperaure, 2.3 eV at −65℃, 2.25 eV at 18℃ and 1.9 eV at 120℃. The lowering of the depth was not observed around the glass transition temperature. On the other hand, it could be observed at 120℃ even below the melting temperature. If the trap is formed by local distortion of molecular arrangement due to crosslinks in the interfacial region between the crystalline and the amorphous part, it is very reasonable that the molecular chain motions liberated in that region erode the traps to lower their depth even below the melting temperature of a crystalline part. Then, the annealing effect of Fig. 48 is explained by the carrier detrapping which is a duplicate process arising from the thermal erosion of the traps by molecular molecular motions and the thermal excitation of carriers in the traps.

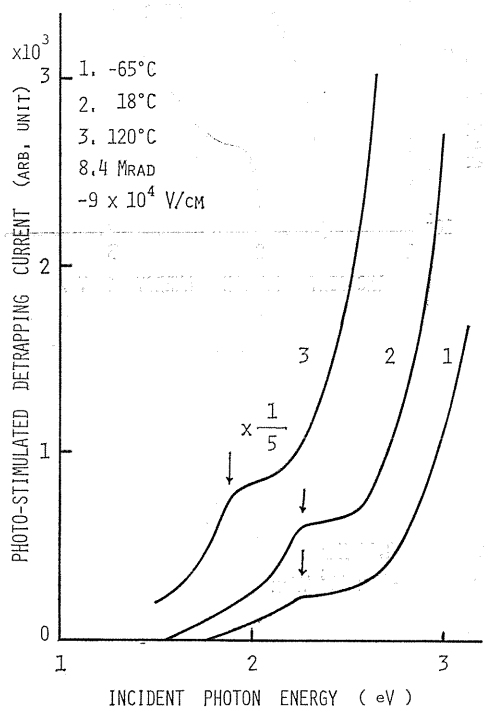

Fig. 53. Temperature dependence of PSDC in γ-irradiated HD-PE.

From the foregoing, it may be concluded that cavity-like traps ascribed to crosslinks in the interfacial region between the crystalline and the amorphous parts are the origin of the deep trap.

The PSDC spectrum of LD-PE γ-irradiated in air below 3.4 eV is now discussed. A tail of PSDC spreads far to a low energy range and an additional peak around 1.3 eV. These traps seem to be concerned with oxidation products such as carbonyl proups. This is supported by the following experiment.

A LD-PE specimen previously oxidized in O_3 ambient was γ-irradiated in vacuum ($\sim 10^{-3}$ Torr). Figure 54 shows the effect of the oxidation on the PSDC spectra. The absorption dosage was limited to 0.016 Mrad in order to excite only carriers but not so greatly to change the chemical structure. Spectrum 1 and 3

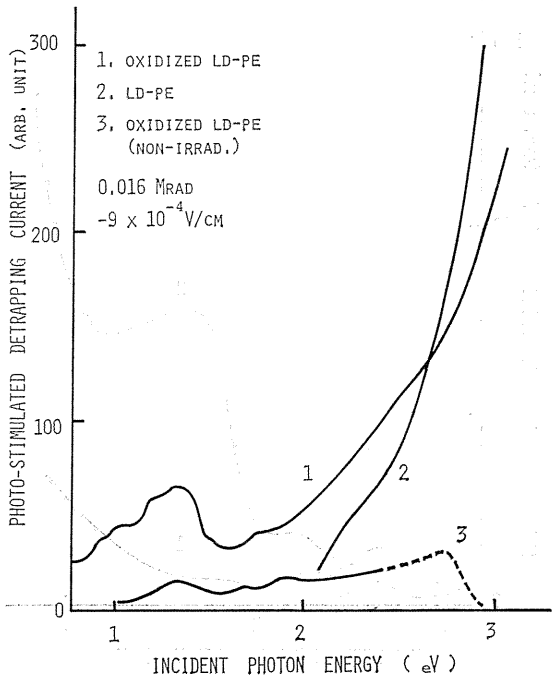

Fig. 54. Effect of oxidation on PSDC in LD-PE.

are results for the oxidized LD-PE γ-irradiated in vacuum and for oxidized LD-PE not irradiated, respectively. A prominent peak around 1.3 eV and also PSDC around 3 eV are enhanced by γ-irradiation. Spectrum 2 is the result obtained for the specimen not previously oxidized but irradiated in vacuum at the same dose. The PSDC spectrum was observed only in the high energy range which was already ascribed to the trap originating from crosslinks.

Similar experiments were carried out on PET. Since PET has been found to show a good photoconductivity, optical excitation of 300 nm in substitution for γ-irradiation was used to fill the traps at -185℃ under various fields E_p, by which photo-excited electrons were drifted into bulk from the illuminated surface. After forming a photoelectret in this way, PSDC spectra were measured by scanning the wavelength of incident light from 3.2 μm to 350 nm and corrected for the light intensity. Figure 55 shows the results of PSDC obtained from the photoelectret formed by illumination at 300 nm under the field E_p of 3.7×10^4 V/cm, and the electret formed by applying only E_p (3.7×10^4 V/cm) without illumination. A peak around 2.3 eV was observed only in the PSDC from the photoelectret, suggesting an existence of deep traps. This peak was found to be thermally cleaned from the results shown in Fig. 56. After measuring PSDC spectrum at -185℃ (curve 1 in Fig. 56), the specimen was heated up to -150℃ and then cooled down to -185℃ to measure PSDC spectrum again. The result is shown by curve 2. Nextly, the specimen was re-heated up to -70℃ over -100℃ at which the peak of TSC from the photoelectret was observed as described later, and cooled down to -185℃. The thermal annealing up to -70℃ was found to eliminate the PSDC peak (curve 3). These PSDC spectra hardly decreased by a repetition of illumina-

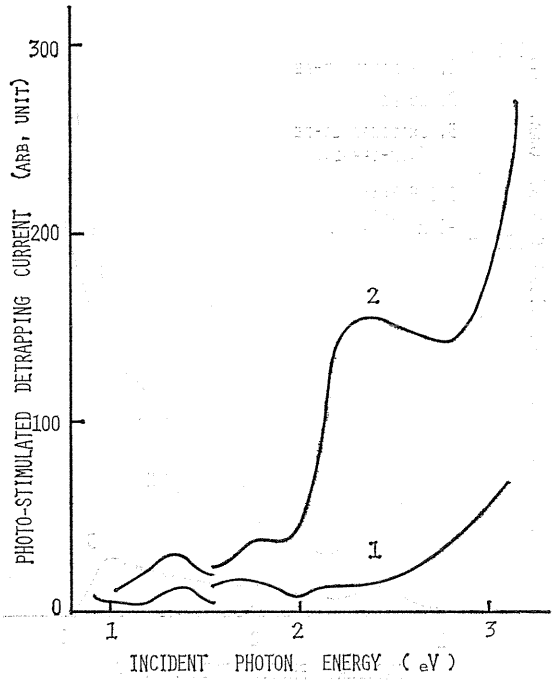

Fig. 55. PSDC spectra in PET obtained from the electret and the photoelectret formed at −185℃, -3.7×10^5 V/cm, with or without illumination, respectively for 2 and 1.

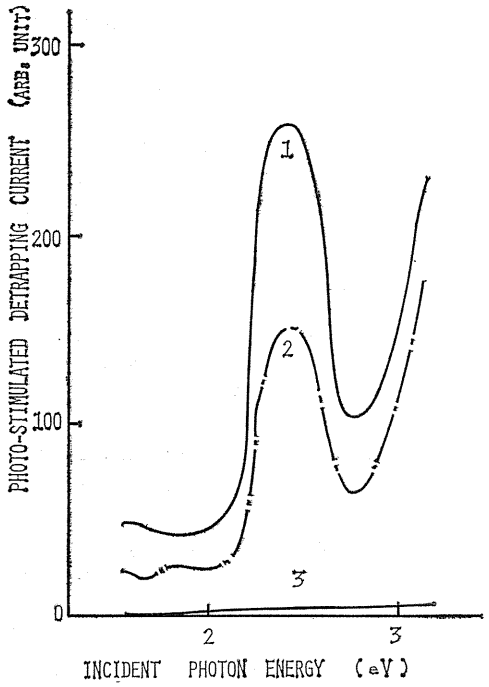

Fig. 56. Thermal quenching of the PSDC spectrum in PET.

tion, because the light intensity was too weak to release considerable amount of trapped carriers.

2) Comparison between Results of PSDC and TSC (TL)

The methods of TSC and TL are convenient means of studying carrier traps. In these methods, the electrical conductitity or light emission from the specimen previously excited with high energy radiation (γ-ray, X-ray, UV light, etc.) at low temperature is measured as the sample is heated at a uniform rate in the dark. The current or light peaks observed during the heating process called "glow curve" are characteristic of thermally detrapped carriers. The temperature at which the current peak appears depends on the trap depth and the heating rate, while the area of the glow curve is concerned with the density of trapped carriers.

Both TSC and TL from PET were measured on the photoelectret formed in the same way as in the case of PSDC measurements. A typical result is shown in Fig. 57. Main peaks appeared around -165℃ and -100℃ denoted P_1 and P_2, respectively, at a heating rate of 6℃/min. A similar experiment was carried out on

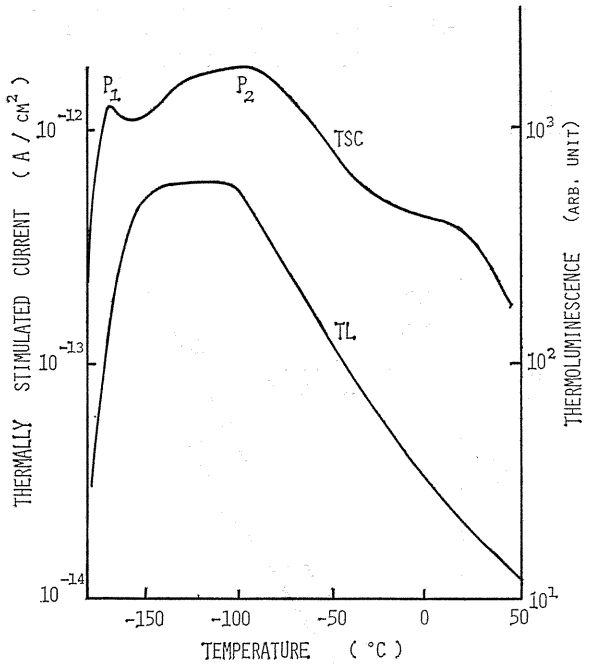

Fig. 57. TSC and TL spectra obtained from the photoelectret of PET.

the electret formed by only an application of the poling field E_p wihtout light. The result is shown in Fig. 58, in which only P_1 peak can be ebserved. The dependence of the peaks P_1 and P_2 on the poling field E_p is shown in Fig. 59 together with the steady state photocurrent. The P_1 peak was proportional to E_p, while P_2 showed a superlinear dependence similar to the steady state photocurrent.

The P_1 peak was found to be independent of the electrode material, the polarity of the poling field E_p. No TL peak corresponding to the P_1 peak was observed, but

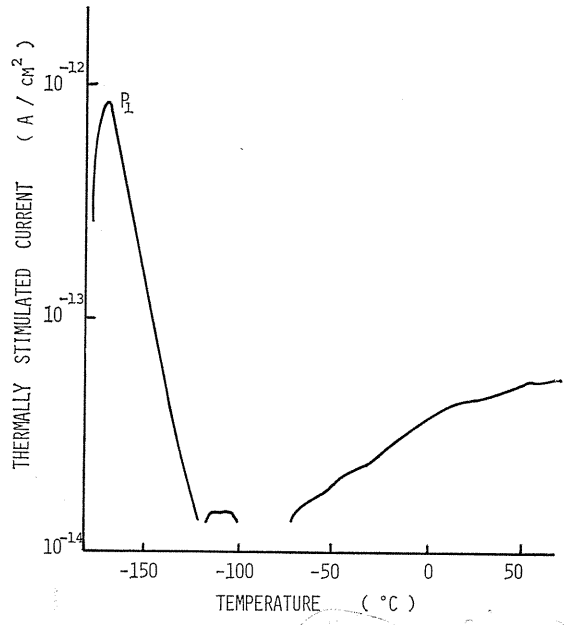

Fig. 58. TSC spectrum obtained from the electret of PET. TL was not observed.

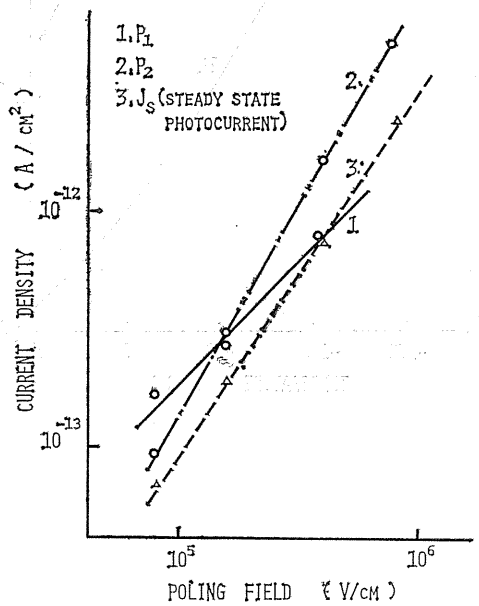

Fig. 59. Dependence of the TSC peaks P_1 and P_2 and steady state photocurrent J_s on the poling field applied to form photoelectrets.

a fairly good correspondence was observed between the TSC peak P_2 and TL peak.

From these experimental results, the P_1 peak and the P_2 peak are considered to be ascribed to the dipole depolarization, and detrapping of photocarriers, respectively. Apparent activation energies estimated by applying the partial heating technique fo the TSC and TL from the photoelectret of PET are shown in Fig. 60. Below -100℃, they were about 0.23 eV, but increased to a somewhat higher value

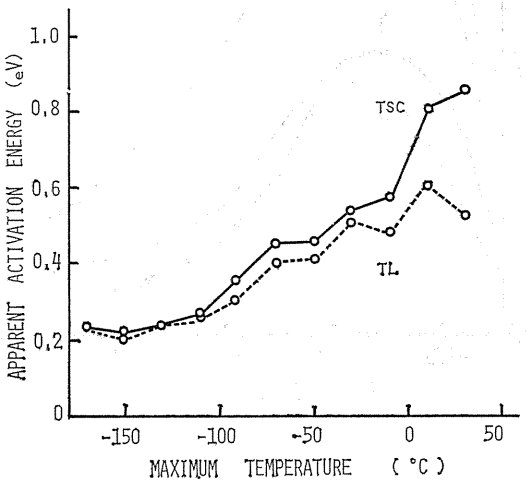

Fig. 60. Apparent activation energies estimated from TSC and TL by the partial heating technique.

of 0.5 eV in the range of $-80 \sim 0$℃, where a prateau of TSC was observed. As mentioned before, the PSDC peak around 2.3 eV was thermally cleaned by up to -70℃ over -100℃ at which TSC P_2 peak appeared. This suggests that TSC and TL peaks (P_2) and PSDC originate from the same trap centers. This is supported also by the result shown in Fig. 61, indicating that both TSC and TL are optically bleached at -185℃, more effectively in the wavelength range of $350 \sim 670$ nm ($3.54 \sim 1.85$ eV). It should be noted that this energy range agrees well with 2.3 eV at which PSDC peak was observed.

There is, however, a great inconsistency between the trap levels estimated from TSC(TL) and PSDC. This can be qualitatively explained from the effect of molecular motions which are peculiar to the polymeric materials. Illers and Breuer[53] reported two peaks of mechanical loss at -105℃ and -70℃ at a frequency of 1 Hz, which are assigned to hindered rotation of two configurations of the COO groups (trans and gauche) with slightly different hindrance potentials. Hsu et al.[54] also reported that the dielectric β relaxation around -70℃ at 30 Hz was the orientation of dipoles of the COO group. The apparent activation energy of the relaxation was estimated at about $0.27 \sim 0.45$ eV in the range of $-150 \sim -100$℃ from the thermally stimulated depolarization current (TSD) analysis,[55] which can evaluate the dielectric relaxation at extremely low frequency by discussing the thermal release of frozen dipoles instead of trapped carriers. It was found that the apparent activation energy for the detrapping of carriers was quite similar to that of

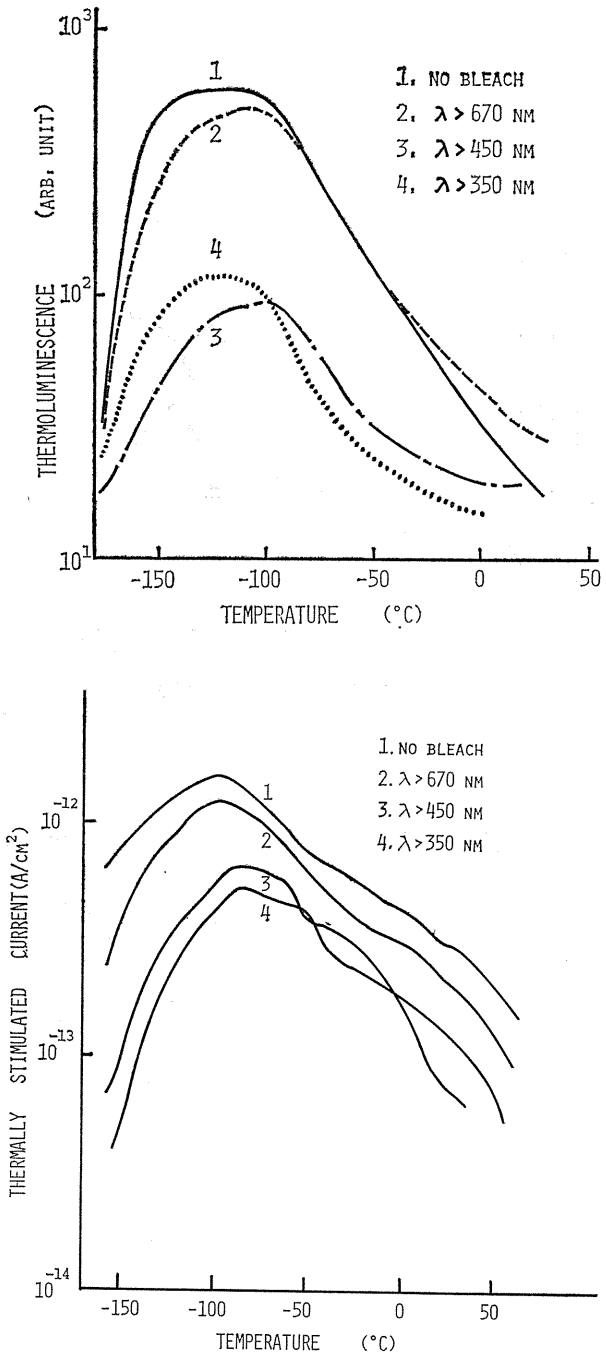

Fig. 61. a) Effect of optical bleach on the TL spectrum. Curves 2, 3 and 4 were obtained by illuminating with light longer than 350, 450 and 670 nm, respecively.
b) Effect of optical bleach on the TSC spectrum.

depolarization of the COO group. This suggests that the detrapping of carriers is enhanced through the erosion or the destruction of the trap center itself by the molecular motions of the COO group. Therefore, the activation energy estimated from the non-isothermal TSC or TL analysis does not coincide with the trap depth optically estimated at −185℃ where molecualr motions of the COO group are not so active. Considering these effects of molecular motions, the origin of the trap may not be any chemical species having higher electron affinity such as O_2 often proposed[39], but physical defects like a cavity or unstable excited species such as radicals beginning to react with each other with the onset of the molecular motion. In other materials such as anthracene, which are not composed of the molecular chains like polymers, the thermally activation energy is found to coincide with the trap depth optically estimated.[56]

3. 3. Photocarrier Transport Mechanism

3. 3. 1. Inter- or intermolecular Transport

The carrier transport phenomena in polymers are often discussed on the ground of the band conduction. As mentioned in § 3. 2. 1, the band structure of polymers, especially linear polymers such as PE has been calculated assuming one dimensional cyclic fields along one molecular chain with infinite length. According to Table 3 in § 3. 2. 1, the forbidden gap of PE lies in 7.7[57] ~ 19 eV[58] and the effective mass is reported to be 0.03 m_e[59] for both electron and hole, and also reported to be 0.5 m_e and 0.37 m_e[60], for electron and hole, respectively, where m_e is the static mass of electron. Recent experimental results on the structure of the valence band proved that the calculated results were not so unreasonable as shown in Fig. 62.[57] In this way, it is not so unreasonable to consider that the band structure

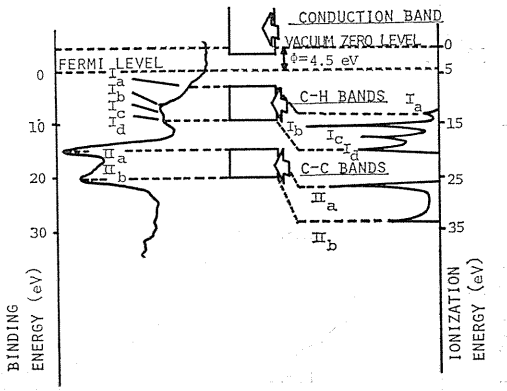

Fig. 62. Band structure of PE reported by J. Delhalle et al.[57]

can be expected at least within the molecular chain. On the other hand, intermolecular bonds are usually sustained by van der Waals force. It seems reasonable to consider that the intermolecular band conduction can hardly be expected. As a consequence, the electrical conduction in polymers is considered to consist of the inter- and intramolecular conduction, and may be limited by either conduction process. Intermolecularly, carriers may hop over or tunnel through the intermolacular

barrier. If it is the case, the intermolecular conduction may be affected by the micro Brownian motion of the molecular chain which is observed around the glass transition temperature T_g.

The temperature dependence of photocurrents in LD-PE is shown in Fig. 63. The photocurrent showed different behaviors in the three temperature regions, namely below -20℃, $-20 \sim 30$℃, and above 30℃. In the low temperature region, photocurrents were nearly independent of temperature, while above 30℃, they increased steeply with temperature. In the internediate region, they showed an

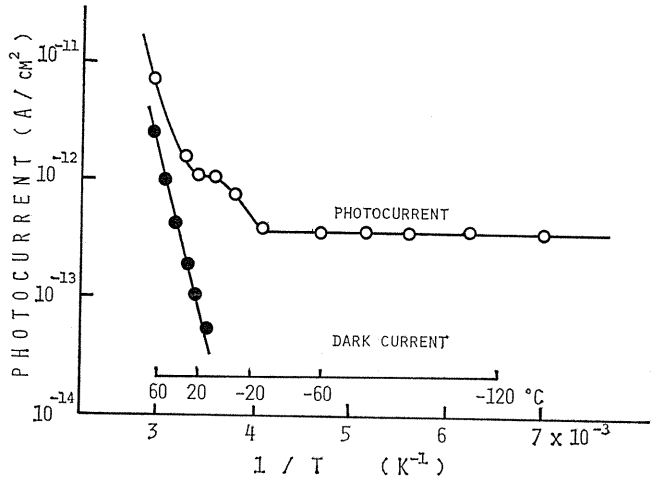

Fig. 63. Temperature dependence of photocurrents in LD-PE (2.5×10^5 V/cm).

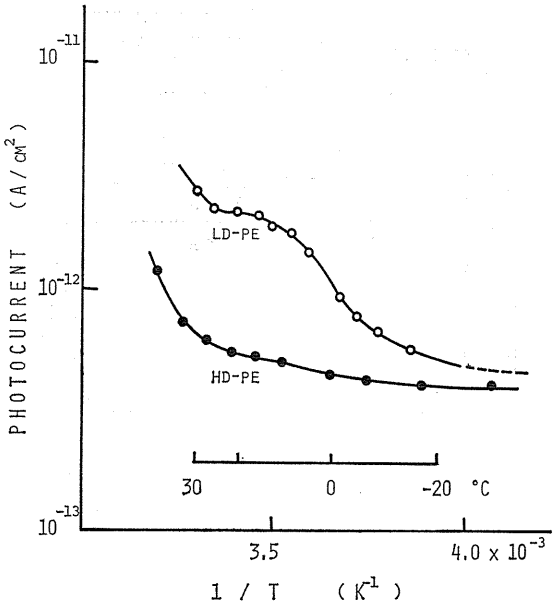

Fig. 64. Temperature dependence of photocurrents in LD-PE and HD-PE in the region from -30 to 30℃.

interesting phenomenon depending on the crystallinity of the specimen. Photocurrents in both HD-PE and LD-PE in this region were measured in more detail (Fig. 64). It is quite clear that a distinct shoulder of photocurrent is observed in LD-PE but scarcely in HD-PE.

This temperature region seems to correspond to the glass transition temperature (β relaxation), which widely distributes by various authors as shown in Fig. 65.[61] The T_g of our specimen of LD-PE were estimated at -15, -39 and -25℃ by the

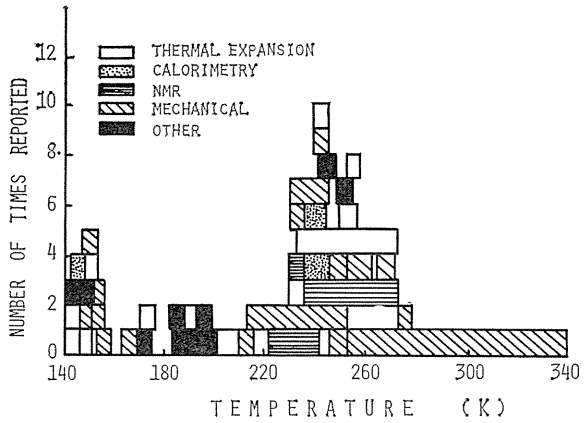

Fig. 65. Summarized results for the glass transition temperature in PE reported by G. T. Davis et al.[61]

capacitance bridge (1 kHz), the Hamon's method (5×10^{-4} Hz)[62] and TSD mentioned before. Flocke[63] has reported that mechanical loss measurements revealed a distinct β loss in LD-PE but not in HD-PE. This is reasonable because the micro Brownian motion of main chains can be released around T_g only in the amorphous part. This coincides with the result of photocurrents shown in Fig. 64, suggesting the micro Brownian motion of molecular chains enhances the intermolecular transport of photocarriers. The liberation of molecular motions in the glass transition region provides more chances for neighboring molecules to approach closely with each other. The width and the height of the intermolecular barrier decrease as the two molecules closely approached and then carriers can more easily tunnel or hop the barrier. It is because the low fraction of the amorphous part in HD-PE that the increase of photocurrent around T_g was not distinctly observed.

Field dependences of photocurrents at three typical temperatures are shown in Fig. 66. Generally, photocurrents were proportional to the applied field at low fields. The departure from the linear dependence took place at higher fields at lower temperature. The plot of log J versus E gives a straight line at high fields and at high temperature (Fig. 67), which is a characteristic of the hopping conduction and the slope of the line gives the barrier height.

The mechanism of the photocarrier transport is schematically shown in Fig. 68. Apparent photocurrents are considered to the sum of the hopping current J_H and the tunneling current J_T. Tunneling currents show an Ohmic behavior at low fields and do not depend on temperature,[64] while hopping currents depend on temperature

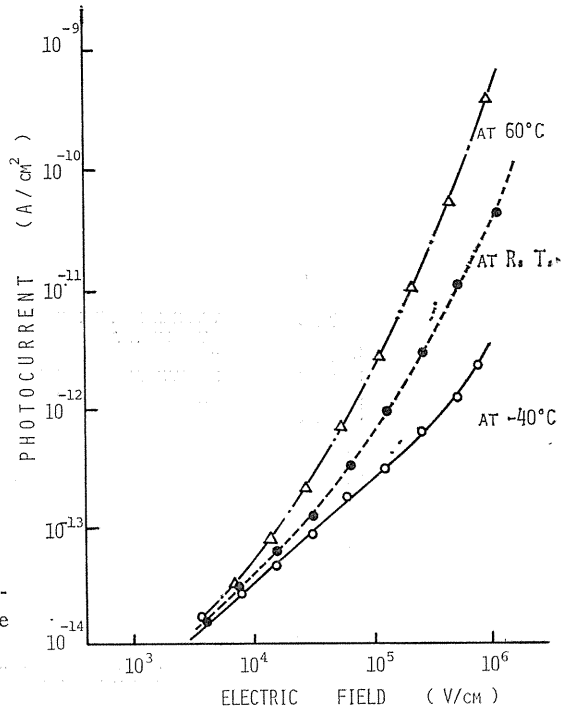

Fig. 66. Field dependence of photocurrents in LD-PE at three temperatures.

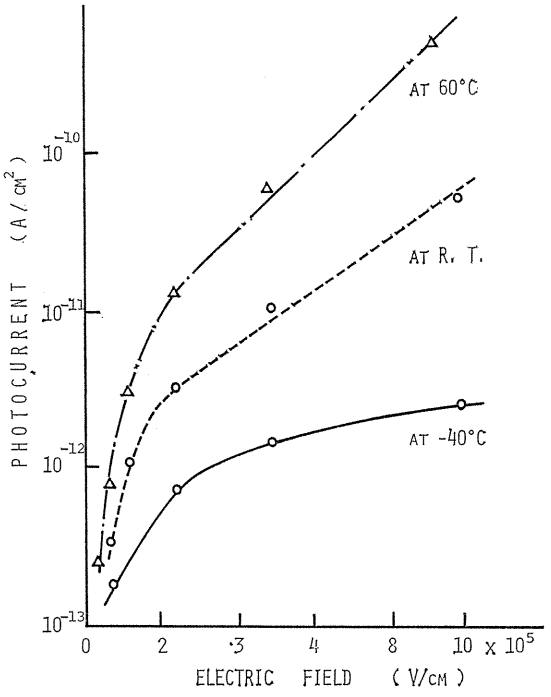

Fig. 67. Log $J-E$ plot of photcurrents in LD-PE.

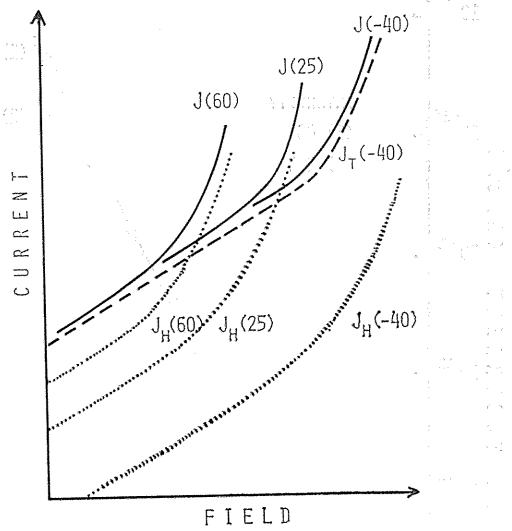

Fig. 68. Model for the photocurrent in LD-PE.

and show an exponential dependence at high fields. At low temperature, J_T prevails at entire field region, but J_H increases as temperature rises and finally above T_g, J_H becomes predominant especially at high fields. At much higher temperature, J_H all the more increases. Consequently the transition field from Ohmic (J_T) to hopping currents shifts towards lower fields. The intermolecular barrier height was estimated from Fig. 67 at 0.7 ~ 1.0 eV at 60℃.

3. 3. 2. Space Charge Limited Photocurrent

Electrical currents induced by carrier injection from electrodes are considered to be either emission limited or bulk limited. Generally, the bulk limited conduction is observed in the material having a low carrier mobility like polymers. The space charge limited current (SCLC) is writtem in the simple case without traps by

$$J=\frac{9}{8}\varepsilon\mu\frac{E_m^2}{d}, \tag{21}$$

where ε is the permittivity of the specimen, μ is the carrier mobility, d is the thickness of the specimen and E_m is the mean (applied) field. The space charge limited current theory is based on the boundary condition that a sufficient carrier reservoir available for injection is maintained at the contact. In the case of photoconductive materials, such reservoir can be maintained by illumination instead of carrier injection from electrodes, because strongly absorbed light produces sufficient density of carriers near the surface. The field strength at the virtual cathode depends on both light intensity and applied field strength, because the carrier density of the contact reservoir is decided by the two opposite processes, *i. e.* the photocarrier generation and the sweep out of carriers from the reservoir by the applied field. Accordingly, at low light intensity, the boundary condition of SCLC may be violated especially at high fields, which makes photocurrents deviate from SCLC.

Experimental results of the photocurrent in PET showed a typical SCLC be-

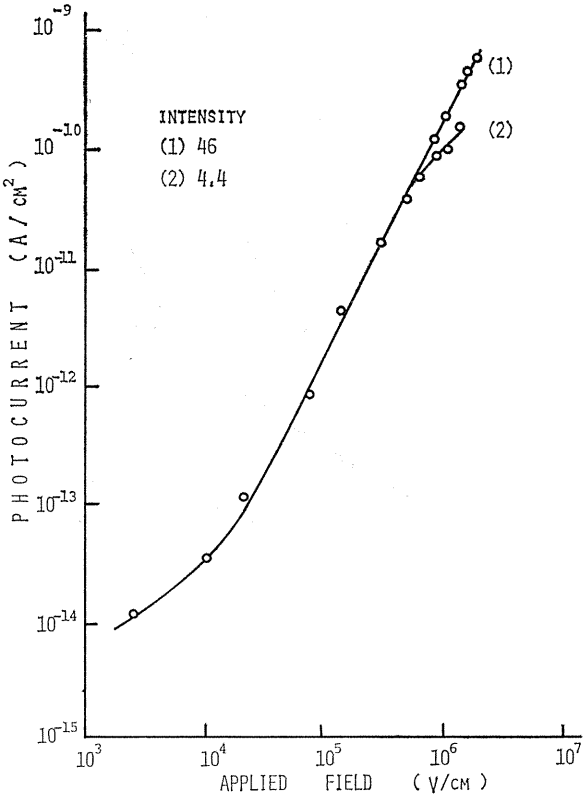

Fig. 69. Field dependence of steady state photocurrents at two light intensities (300 nm).

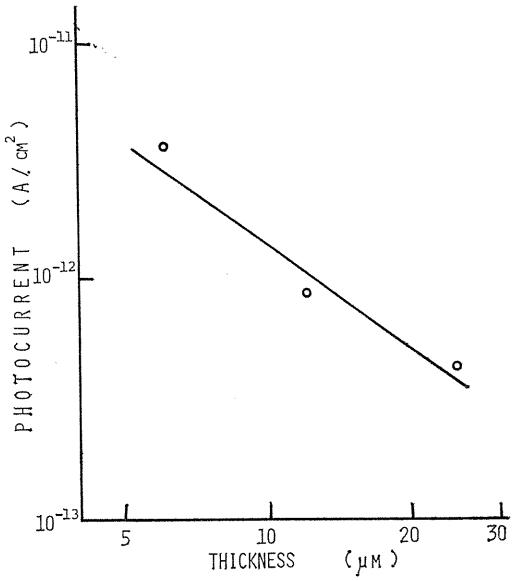

Fig. 70. Thickness dependence of photocurrents in PET (-1.6×10^{5}V/cm, 300 nm).

havior as indicated in Figs. 69 and 70. The steady state photocurrent was proportional to the square of the applied field E_m at high light intensity, but at low light intensity it deviated from the square law at high fields and it also depended on film thickness. These behaviors are qualitatively explaind from the SCLC theory. If it is the case, the photocurrent in the steady state should not depend on the light intensity because of the bulk limited conduction. This was experimentally observed as shown in Fig. 71.

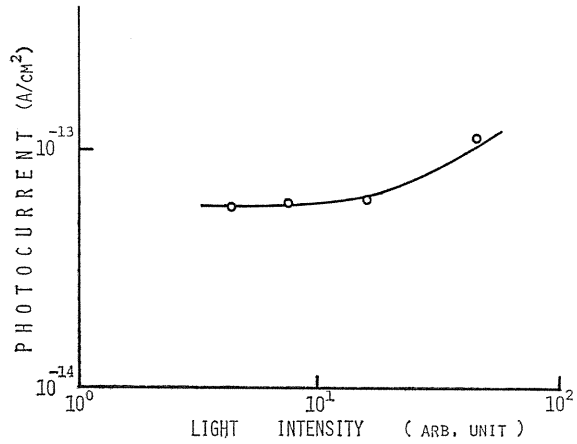

Fig. 71. Intensity dependence of photocurrents in PET (-3.7×10^4 V/cm, 300 nm).

The deviation from the square law observed at low light intensity at high fields is explained from the model of the electrical conduction whith an insufficient reservoir developed by Croitoru.[65] Neglecting the diffusion current and considering the steady state one carrier conduction, the current density J and mean electric field E_m can be expressed by

$$J=\left(\frac{\varepsilon\mu}{d}\right)E_m^2\sigma, \tag{22}$$

$$E_m=E(d)\eta^{-1}, \tag{23}$$

where $E(d)$ is the cathode field strength and non-dimensional variables σ and η satisfy the following relation

$$3\sigma=(\eta^2+2\sigma)^{3/2}-\eta^3. \tag{24}$$

The relation between σ and η^{-1} was calculated from equation 24) as shown in Fig. 72. For high η^{-1}, σ is approximately equal to 9/8. Then, equations 22) and 23) are reduced to

$$J=\left(\frac{\varepsilon\mu}{d}\right)E_m^2\frac{9}{8}, \tag{25}$$

$$E_m\gg E(d). \tag{26}$$

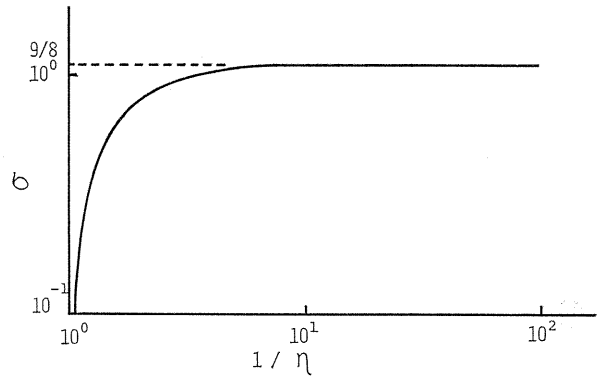

Fig. 72 Correction factor σ as a function of the ratio of the mean field to the cathode field ($1/\eta$).

This corresponds to a simple SCLC case.

When the cathode field becomes comparable to the applied field by some causes like a lowering of light intensity, η^{-1} approaches to 1.0, then σ decreases from 9/8. Therefore, the photocurrent decreases from SCLC given by equation 25) to the current expressed by equation 22) at high fields.

The correction factor σ for the steady state photocurrent at low light intensity at a certain E_m can be evaluated as shown in Fig. 73 from results of Fig. 69 by taking the ratio of the photocurrent at low light intensity to that at high light intensity. The value of σ is nearly constant (9/8) at low fields but decreases at high fields.

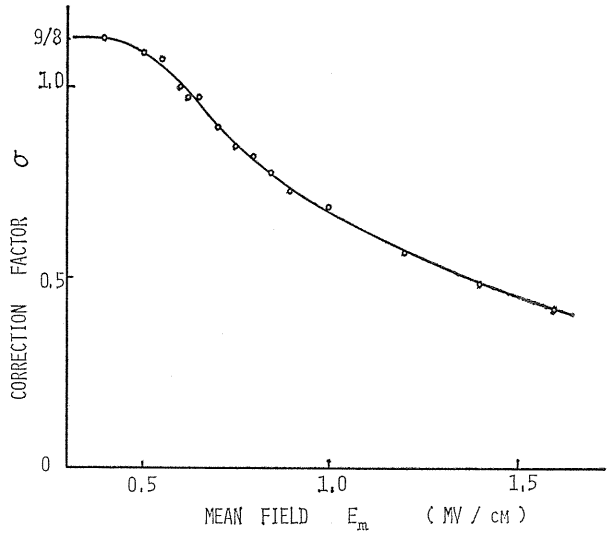

Fig. 73. Correction factor σ as a function of the mean field E_m.

The cathobe field $E(d)$ can be estimated from equation 23) by evaluating η for each σ. The result is shown in Fig. 74. At high fields but lower than 5×10^5 V/cm, cathode field $E(d)$ can be neglected as compared with the mean field E_m. The cathode field at $E_m=10^6$ V/cm is shown to be 6×10^5 V/cm, which is fairly close to the mean field. Accordingly the SCLC condition can not be sustained at such high fields.

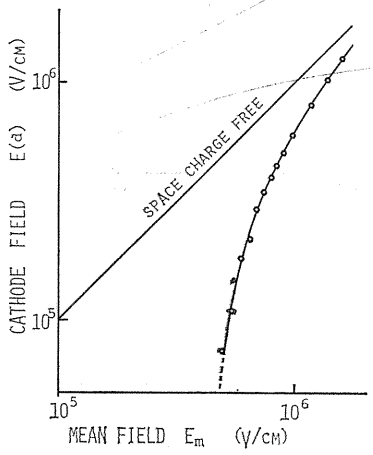

Fig 74 Cathode field at each mean field E_m.

The spatial distribution of the electric field and the carrier density can be also estimated from results of Figs. 73) and 74) by the following equations

$$E(x)=[E(d)^2+2E_m^2\sigma(1-x/d)^{-1}]^{1/2}, \tag{27}$$

$$N(x)=\frac{\sigma\varepsilon}{qd}E_m^2E(x)^{-1}. \tag{28}$$

Typical results are shown in Figs. 75 and 76 at $E_m=10^5$ V/cm and 10^6 V/cm for the case of low light intensity. At $E_m=10^5$ V/cm, the cathobe field $E(x)$

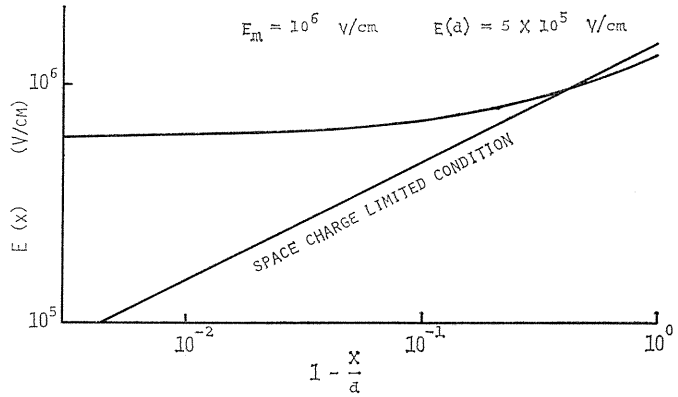

Fig. 75. Spatial distribution of the field with the poor contact reservoir.

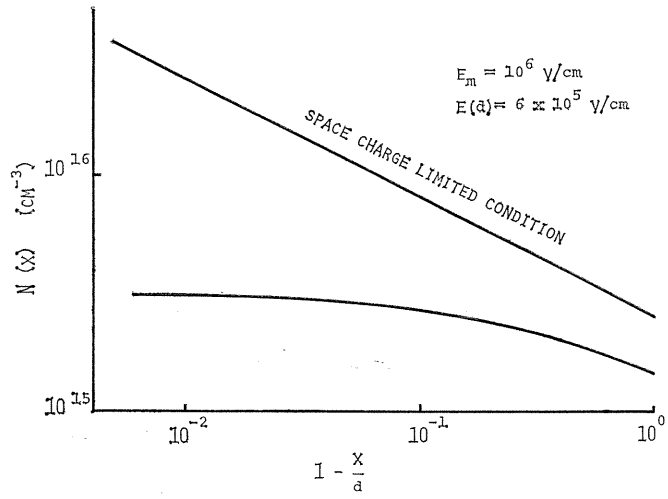

Fig. 76. Spatial distribution to the carrier density with the poor contact reservoir.

increases with the square root of spatial coordinate x as expected from the SCLC theory. On the other hand, at $E_m = 10^6$ V/cm, $E(x)$ is much higher than the field strength expected for SCLC, especially near the cathode.

Similarly the carrier density $N(x)$ decreases with the inverse square root of x at $E_m = 10^5$ V/cm where the space charge limited condition is satisfied, whereas at $E_m = 10^6$ V/cm $N(x)$ near the cathode is apparently less than that required to maintain SCLC. The carrier density estimated from these calculations is approximately of the order of 10^{15} cm^{-3} under our experimental condition, which is not so unreasonable in polymers.

Since the above discussion is based on a simple trap-free theory, it is necessary as a next step to take traps in PET into account. The theory of SCLC with a single set of shallow traps is characterized by a ratio of free to trapped carriers, θ.[66] Then, Poisson's equation is reduced to

$$\frac{dE}{dx} = -\frac{qn}{\varepsilon\theta}. \tag{29}$$

Therefore, all equations inferred above can be applied also to the case with shallow traps if only ε is replaced by $\varepsilon\theta$. The obtained results in Figs. 73 ~ 76 do not require any serious corrections. Further understanding of traps in PET will be required for a more complete discussion of the experimental results.

4. Conclusion

The investigation of the electronic conduction in polymers has made great progress by the analysis of photoconduction. Since surface properties such as contact barrier height and surface states greatly affect the insulation properties of polymers, it is quite necessary to understand the the surface phenomena in more detail. The result of photoinjection from electrodes could give many useful informations on the surface

phenomena which has scarcely been discussed to date.

Another serious factor affeting the insulation property is the space charge. It distorts an electric field pattern within polymers and often leads to an dielectric breakdown of solids. The study of carrier traps has been intensively conducted by analyses of TSC and TL giving wide interesting information about the space charge, but these analyses have an imperfection originating from their nonisothermal properties. The isothremal technique of PSDC analysis firstly applied to polymers could show an intimate correlation between the detrapping process and the molecular motion. The trapping parameters such as energy levels were found to be seriously affected by the molecular motion.

The carrier transport in polymers was also affected by the molecular motion as observed in the anomalous temperature dependence of photocurrent in LD-PE which can be understood from the enhanced intermolecular conduction by the molecular motion around the glass transition temperature. In this way, it can be said that molecular motion is a most important factor for understanding the electrical conduction in polymers.

The exciton induced or intrinsic photoconduction in polymers has not intensively been investigated yet. The investigation of the electronic structure of polymers is all the more important to understand the fundamental properties of polymers. Further work should be accumulated.

Aknowledgement

The authers wish to express their thanks to Messrs T. Ueno, T. Osawa, T. Ina anp K. Mori for their coorperation in carrying out the experiments. They also wish to express their thanks to Prof. G. Sawa (Mie University) for his instructive discussions. They also thank to Prof. K. C. Kao (Manitoba University), who stayed at Nagoya University for a month during his sabbatical year, for his kind instruction. They thank to Messrs K. Itakura and N. Yamada (Mitubishi Petrochemical Ind. Ltd.) and Mr. I. Ouchi (Teijin Co. Ltd.) for supplying specimens.

This work was partly supported by the Grand-in-Aid for Scientific Research from the Ministry of Education.

References

1) J. D. Comins and H. J. Wintle; J. Polymer Sci.: Polymer Phys. Ed. **10** (1972) 1368.
2) Y. Takai, T. Osawa, T. Mizutani and M. Ieda; Japan. J. Appl. Phys. **14** (1975) 473.
3) M. Kryszewski, A. Szymanski, A. Wlochowicz; J. Polymer Sci. **C 16** (1968) 3921.
4) A. Hersping and A. Oster; Kolloid-Z. u. Z. Polymere **226** (1968) 103.
5) T. Mizutani, Y. Takai and M. Ieda; Japan. J. Appl. Phys. **11** (1971) 411.
6) J. F. Fowler; Proc. Roy. .Soc. (London) **A 236** (1956) 464.
7) G. Oster, G. K. Oster and M. Kryszewski; Nature **191** (1961) 164.
8) H. J Wintle and A. Charlesby; Photochem. and Photobio. **1** (1962) 231.
9) T. Tanaka and Y, Inuishi; Japan. J. Appl. Phys. **6** (1967) 1371.
10) R. H. Partrige; J. Chem. Phys. **45** (1966) 1685.
11) K. J. Less and E. G. Wilson; J. Phys. C: Solid State Phys. **6** (1973) 3110.

12) Yu. A. Cherkasov, L. N. Vinokurova, O. M. Sorokin and V. A. Blank; Soviet Phys.-Solid State **11** (1970) 1590.
13) R. A. George, D. M. Martin and E. G. Wilson; J. Phys. C: Solid State Phys. **5** (1972) 871.
14) T. Tanaka; J. Appl. Phys. **44** (1973) 2430.
15) W. L. McCubbin; J. Chem. Phys. **43** (1965) 983.
16) M. H. Wood, M. Bareber, I. H. Hiller and J. M. Thomas; J. Chem. Phys. **56** (1972) 1788.
17) L. Doub et al.; J. Am. Chem. Soc. **69** (1947) 2714.
18) S. Nagakura and J. Tanaka; J. Chem. Phys. **22** (1954) 236.
19) J. Petruska; J. Chem. Phys. **34** (1961) 1120.
20) M. Leibowitz and A. Weinreb; J. Chem. Phys. **46** (1967) 4652.
21) A. Itaya, K. Okamoto and S. Kusabayashi; Bull. Chem Soc. Japan **49** (1976) 2082.
22) M. T. Vala, Jr., J. Haebig, and S. A. Rice; J. Chem. Phys. **43** (195) 886.
23) M. Nowakowska, J. Najbard and B. Waligóra; Europ. Polymer J. **12** (1976) 387.
24) K. Okamoto, S. Kusabayashi and H. Mikawa; Bull. Chem. Soc. Japan **46** (1973) 2324.
25) A. Fort and A. Coret; J. Chem. Phys. **62** (1975) 3269.
26) Y. Takai, T. Osawa, T. Mizutani and M. Ieda; J. Polymer Sci. **15** (1977) 945.
27) H. Bauser and W. Klöpffer; Chem. Phys. Letters **7** (1970) 137.
28) H. B. Devore; Phys. Rev. **102** (1956) 86.
29) A. E. Binks, A. G. Campbell and A. Sharples; J. Polymer Sci. **A-2** (1970) 529.
30) J. H. Ranicar and R. J. Fleming; J. Polymer Sci. **A-2** (1972) 1321.
31) H. J. Wintle and G. H. Tibensky; J. Polymer Sci.: Polymer Phys. Ed. **11** (1973) 25.
32) R. A. Wallace; J. Appl. Polymer Sci. **17** (1973) 231.
33) D. K. Davies; J. Phys. D: Appl. Phys. **2** (1969) 1533.
34) H. B. Bauser, W. Klöpffer and Rabenhorst; *"Advance in Static Electricity"* vol. 1. (1970) (Brussels: Auxilia) pp 2-9.
35) H. Krupp; *"Static Electrification"* (London: Institute of Physics and the Physical Society) pp 1-16.
36) D. M. Talor and T. J. Lewis; J. Phys. D: Appl. Phys. **4** (1971) 1346.
37) A. M, Goodman; J. Electrochem. Soc. **115** (1968) 276.
38) A. M. Cowley and S. M. Sze; J. Appl. Phys. **36** (1965) 3212.
39) W, Knappe, H. U. Schrenker and A. Zybail; Kolloid-Z. Z. Polymere **250** (1972) 1135.
40) K. Amakawa and Y. Inuishi; J. I. E E. Japan **93-A** (1973) 533 [in Japanese].
41) D. K. Davies; J. Phys. D: Appl. Phys. **5** (1972) 162.
42) I. Boustead and A. Charlesby; Proc. Roy. Soc. (London) A **316** (1970) 291.
43) R. H. Partridge; J. Polymer Sci. **A-3** (1965) 2817.
44) A. Van Rogan; Annual Report-Conference on Electrical Insulation and Dielectric Phenomena (NAS, Washington D. C., 1965) p 3.
45) J. Jortner; Radiat. Res. Suppl. **4** (1964) 24.
46) G. N. Patel and A. Keller; Polymer Letters Ed. **11** (1973) 737.
47) H. Kashlwabara and K. Shinohara; J. Polymer Sci. **15** (1960) 1129.
48) P. Alexander and D. Toms; J. Polymer Sci. **22** (1956) 343.
49) J. P. Luongo and R. Salovay; J. Appl. Polymer Sci. **7** (1963) 2307.
50) E. J. Lawton, J. S. Balwit and R. S. Powell; J. Polymer Sci. **32** (1958) 257.
51) M. Kondo and M. Dole; J. Phys. Chem. **70** (1966) 883.
52) G. N. Patel and A. Keller; J. Polymer Sci.: Polymer Phys. Ed. **13** (1975) 303.
53) K. H. Illers and H. Breuer; J. Colloid Sci. **18** (1963) 1.
54) B-S. Hsu and S-H. Kwan; J. Polymer Sci.: Polymer Phys. Ed. **14** (1976) 1591.
55) T. Hino and Y. Kitamura; J. I. E. E. Japan **95-A** (1975) 71 in [Japanese].
56) H. Kokado and W, G, Schneider; J. Chem. Phys. **40** (1964) 2937.
57) J. Delhalle, J. M. Andre, S. Delhalle, J. J. Pireaux. R. Caudano and J. J. Verbist; Chem. Phys. Letters **23** (1973) 206.
58) B. J. Duke and B. O'Leary; Chem. Phys. Letters **20** (1973) 459.

59) J. E. Falk and R. J. Fleming ; J. Phys. C ; Solid State **6** (1973) 2954.
60) W. L. McCubbin ; J. Polymer Sci. **C-30** (1970) 181.
61) G. T Davis and R. K. Eby ; J. Appl. Phys. **44** (1973) 4274.
62) B. V. Hamon ; Proc. I. Elec. Eng. Pt-4 **99** (1952) 151.
63) H. A. Flocke ; Kolloid Z. **180** (1962) 118.
64) D. R. Lamb ; *"Electrical Conduction Mechanisms in Thin Insulating Films"* (Matheuen and Co. Ltd. London 1967) p 56.
65) Z. Croitoru ; *"Progress in Dielectrics* 6" (Heywood, London 1965) p 103.
66) M. A. Lampert and P. Mark ; *"Current Injection in Solids"* (Academic Press, Inc. 1970).